CONTROLS ANALYSIS OF NUCLEAR ROCKET ENGINE AT POWER RANGE OPERATING CONDITIONS

by Dale J. Arpasi and Clint E. Hart

Lewis Research Center
Cleveland, Ohio

CONTROLS ANALYSIS OF NUCLEAR ROCKET ENGINE

AT POWER RANGE OPERATING CONDITIONS

By Dale J. Arpasi and Clint E. Hart

Lewis Research Center
Cleveland, Ohio

NATIONAL AERONAUTICS AND SPACE ADMINISTRATION

CONTROLS ANALYSIS OF NUCLEAR ROCKET ENGINE
AT POWER RANGE OPERATING CONDITIONS

by Dale J. Arpasi and Clint E. Hart

Lewis Research Center

SUMMARY

Techniques used to evaluate the dynamics of a nuclear rocket engine for control purposes are presented. A linear analysis, applied to transfer functions describing a NERVA-type engine at various operating conditions, was used to develop stable engine control in the power range of operation. The power range of operation is defined as that region of engine operation above 1-percent reactor power and 10-percent propellant weight flow. The effects of operating level and reactor period on the engine dynamics were considered in the analysis by investigating these dynamics at four engine operating levels and three reactor periods.

Exhaust-nozzle chamber temperature and pressure were considered the primary engine variables to be controlled because of their relation to the engine specific impulse and thrust. Two methods of temperature control were investigated in terms of system dynamics: (1) the use of an inner-reactor-power control loop manipulated by a temperature controller and (2) direct manipulation of the control drums by the temperature controller with no direct control of reactor power.

The results indicated that slightly better bandwidths could be achieved with the use of an inner-power loop. The power loop partly eliminated the restrictions imposed on the gain of the temperature controller by the effects of reactor period, thus allowing increased temperature-loop bandwidth. The effects of operating level on the response of the temperature loop were diminished by the use of adaptive-gain control. The linear analysis at the various operating levels was used to obtain a functional relation between the controller gain and chamber pressure for use in an adaptive controller.

The analytically derived controllers for the various loops were used to control the nonlinear engine simulation. The closed-loop frequency response of the controlled simulation was in close agreement with the analytically derived response, lending verification to the analysis. Transient characteristics of the controlled engine simulation were obtained for nominal power range startups.

INTRODUCTION

The feasibility of space vehicle propulsion through the use of nuclear energy is being demonstrated in the NERVA program. Many design problems have been overcome, and startup and extended operation of a complete engine have been achieved. Tests on actual engine prototypes and on computer simulations have produced data describing the steady-state and dynamic behavior of the engine. These data have been used to develop preliminary designs of engine control systems (ref. 1).

A simplified diagram of a NERVA-type engine is presented in figure 1. The engine operates on a bootstrap principle. Propellant from the storage tank is pumped into the reflector through coolant tubes in the exhaust nozzle. From the reflector the propellant flows through the reactor core, where it is heated, and then it is expelled at high temperature into the exhaust-nozzle chamber and expanded through the nozzle to produce thrust. Part of the heated propellant in the nozzle chamber is bled off and mixed with cooler fluid emerging from the reflector. This mixture is fed through the turbine-power-control valve to drive the turbine, which, in turn, drives the pump. The control drums are used to vary the amount of poison in the reactor, thereby increasing or decreasing reactor power and, consequently, the amount of heat transferred to the propellant.

The thrust and specific impulse of the engine are of primary concern. For choked flow through the exhaust nozzle, these parameters are proportional to chamber pressure and chamber temperature, respectively. The control of chamber pressure, and consequently, thrust may be accomplished by manipulating the turbine-power-control valve. Two methods are considered for use in the control of chamber temperature or specific impulse:

(1) The use of an inner-reactor-power control loop manipulated by a temperature controller

(2) Direct manipulation of the control drums by the temperature controller without closed-loop control of the reactor power

Because of the complex nature of the engine, evaluation of these concepts over the range of engine operating conditions is extremely difficult. A complete analysis leading to the development of an optimum design of engine control has not been accomplished, and it is for this reason that the present investigation was initiated. This investigation was conducted specifically

(1) To define further the characteristics of engine control systems necessary to permit wide-range operation of the engine

(2) To compare, in terms of engine dynamics, the two types of chamber temperature control

(3) To investigate the possibility of using adaptive control techniques in improving system response over the range of operating conditions

2

(4) To design engine controllers that would permit stable operation of the engine over a wide range of operating conditions

SYMBOLS

l	operating level
P	exhaust-nozzle chamber pressure, psi
Q	reactor power, Btu/sec
Q_o	reference power, Btu/sec
s	Laplace transform variable, $\sec^{-1}$
T	exhaust-nozzle chamber temperature, $^O R$
t	time, sec
$\dot{w}$	weight flow rate through reactor core, lb/sec
δk	total reactivity
δk_D	control-drum reactivity
δk_I	inherent reactivity feedback
θ_D	control-drum angle, deg
θ_v	turbine-power-control valve angle, deg
τ	reactor period, sec
ω	frequency, rad/sec

Subscripts:

d	demand
e	error
m	measured
m'	compensated measured

Transfer function notations:

$G_{c,p}$	power controller, $\Delta\theta_{D,d}/\Delta \log(Q_e/Q_o)$, deg
$G_{c,pr}$	pressure controller, $\Delta\theta_{v,d}/\Delta P_e$, deg/psi
$G_{c,t}$	temperature controller (with inner-power loop), $\left[\Delta \log(Q_d/Q_o)\right]/\Delta T_e$

G_D	control drums and actuators, $\Delta\delta k_D/\Delta\theta_{D,d}$, $\deg^{-1}$
G_p	closed power loop, $\Delta Q/[\Delta \log(Q_d/Q_o)]$, Btu/sec
G_{pr}	closed pressure loop, $\Delta P/\Delta P_d$
G_r	reactivity loop, $\Delta Q/\Delta\delta k_D$, Btu/sec
$G_{s,pr}$	heat-transfer and flow system (pressure), $\Delta P/\Delta\theta_v$, psi/deg
$G_{s,t}$	heat-transfer and flow system (temperature), $\Delta T/\Delta Q$, $(^{\circ}R)(sec)/Btu$
G_t	closed temperature loop, $\Delta T/\Delta T_d$
G_{th}	thermocouple, $\Delta T_m/\Delta T$
$G_{th,m'}$	thermocouple compensation, $\Delta T_{m'}/\Delta T_m$
G_v	turbine-power-control-valve actuators, $\Delta\theta_v/\Delta\theta_{v,d}$
H	heat-transfer and flow system (inherent reactivity), $\Delta\delta k_I/\Delta Q$, sec/Btu
K_c	controller gain
K_{pr}	pressure sensor
K_s	reactor power sensor, $[\Delta \log(Q_m/Q_o)]/\Delta Q$, sec/Btu

METHOD OF ANALYSIS

A controls analysis utilizing linear techniques, such as Bode plots and root-locus diagrams, was performed on the analog computer simulation of a NERVA-type nuclear rocket engine. This simulation, along with the development of the transfer functions used as input data for this analysis, is described in detail in reference 2. These transfer functions were obtained by measuring the response of a controlled variable to its respective manipulated variable, while the other manipulated variable was held constant; that is, transfer functions relating chamber temperature to reactor power and reactor power to control-drum reactivity are developed at constant turbine-power-control valve angle. These are used in this analysis to derive temperature and power controllers. The transfer functions relating chamber pressure and turbine-power-control valve angle are also developed, in reference 2, at constant control-drum reactivity. However, when these transfer functions were used in developing controller compensation for the pressure control loop, they did not yield good results. They did not accurately describe the relation of the chamber pressure to the turbine-power-control valve angle when a control loop was closed around the chamber temperature. Thus, a strong cross-coupling was indicated between the chamber pressure and the control drums; consequently, it was necessary to develop a controller for the chamber temperature and then to determine the

4

relation between pressure and turbine-power-control valve angle at a constant temperature demand. Further discussion of this subject is presented in the section CHAMBER-PRESSURE CONTROL.

The nonlinearities of the engine make its dynamics subject to the operating level and the reactor period. To account for the level effects, transfer functions were determined at four engine steady-state operating levels that were intended to give a fair representation of engine dynamics over the power range of operation. These levels are illustrated in the steady-state operating map of figure 2, where chamber temperature is plotted against chamber pressure at various values of the manipulated variables. Level I is the design level of the engine.

The effects of reactor period on the reactor transfer function are described in reference 3. These effects were taken into account by analyzing the system at infinite and 2- and 0.5-second reactor periods.

The open-loop transfer functions of the various control loops were implemented on a potential plane analog computer to obtain open-loop Bode plots of the system in question without a controller. These plots along with a knowledge of the pole-zero locations of the open-loop transfer functions were used in determining a controller configuration for each loop. (Descriptions of the ESIAC Potential Plane Analog Computer and the log s plane, in which much of this analysis was done, are given in refs. 4 and 5.)

A wide bandwidth with adequate stability and damping of the loop response was used as the design criteria for controller configuration and gain. A type I controller was required in each loop (i.e., required integration for zero steady-state position error). Lead and lag terms were added to the control configuration at frequencies that would improve the bandwidth or stability of the loop, as indicated by the Bode plots and pole-zero diagrams. Consideration of component saturation (such as the controller amplifier and the drum and valve actuators) due to lead terms and high gains in the controller also influenced the choice of design. The effects of large-scale input perturbations were not considered in the controller evaluation, however, since the immediate objective of the analysis was to provide adequate response to ramped demand schedules, as might be encountered in normal engine operation.

Engine constraints, such as the tie-rod temperature limit and the minimum reactor period limitations, were not given consideration in the choice of the controller. Wide bandwidth response (a measure of the ability of the output variables to track their demand signals) is desirable in all safe operating conditions of the engine. Variables indicating unsafe operating conditions must be sensed and used to apply nonlinear restrictions, such as clamping or switching, to the wide bandwidth controller to avoid the unsafe conditions. Investigations of this sort were considered as being outside the scope of this linear analysis.

After a control configuration was decided on, system stability for various controller

gains was determined by observing the open-loop phase and gain margins at the operating levels and periods under consideration. Dominant pole-damping ratios, obtainable from root-locus plots generated on the potential plane computer, were used as indications of the magnitude of any closed-loop resonances. Once a controller gain was determined, these plots were used to provide the poles of the closed-loop transfer function.

When a suitable controller was obtained, it was used to control the analog simulation. Closed-loop frequency responses were then taken at the four operating levels and compared with the analytically derived closed-loop responses to verify the linear analysis. This process was repeated for each control loop. When controllers for all loops were obtained, power range startup transients were run on the analog simulation to check the overall behavior of the controllers.

REACTOR POWER CONTROL

System Description

A block diagram of the power control loop is presented in figure 3. The controller accepts an error signal and converts it to an angle demand $\theta_{D,d}$ for input to the control-drum actuators. The actuator response was represented by a second-order lag with a natural frequency of 25 radians per second and a damping ratio of 0.5. The equation used to relate control-drum angle θ_D to control-drum reactivity δk_D is

$$\delta k_D = 0.06864 \sin^2 \frac{\theta_D}{2} - 0.03432$$

The gain term associated with this relation is therefore

$$\frac{\Delta \delta k_D}{\Delta \theta_D} = \frac{d \delta k_D}{d \theta_D} = 5.99 \times 10^{-4} \sin \theta_D$$

In the block diagram (fig. 3), this gain is lumped into the actuator transfer function.

The relation of reactor power to control-drum reactivity is also shown in the block diagram of figure 3. Reactor power Q and turbine-power-control valve angle θ_v act through the heat-transfer and flow system to determine the inherent reactivity δk_I in the reactor. Transfer functions that are dependent on operating level were derived to relate δk_I to Q at constant θ_v. These transfer functions were then used in conjunction with the period-dependent transfer functions of the reactor kinetics to form the transfer function of the inherent reactivity loop.

6

The reactor power sensor (fig. 3), assumed to be a logarithmic gain with negligible dynamics, produces a measured log-power signal, which is summed with the log-power demand signal to provide the error input to the power controller. The gain of the sensor is given by

$$K_s = \frac{d \log_{10} \frac{Q}{Q_o}}{dQ} = \frac{\log_{10}e}{Q} = \frac{0.43429}{Q}$$

Open-Loop Dynamics

The dynamics of the open power loop (at constant θ_v), excluding controller dynamics, may be expressed in transfer-function form as

$$\left. \frac{\Delta \log \frac{Q_m}{Q_o}}{\Delta \theta_{D,d}} \right|_{\theta_v} = K_s G_D G_r$$

This transfer function exhibits dependency both on operating level and on reactor period. Values for K_s, G_D, and G_r are given in table I at the reactor periods and operating levels under consideration.

The Bode plots of figure 4 illustrate the reactor-period effects on the open-power-loop response at level I. These effects are typical of the other levels. Figure 4(b) indicates that, at frequencies above 12 radians per second, the minimum phase angle occurs at the shortest reactor period. The dynamic gain of the transfer function $\left[\Delta \log(Q_m/Q_o)\right]/\Delta \theta_{D,d}$ is also a maximum at the shortest period. These facts indicate that the least stable conditions of the loop occur at the short reactor periods. It therefore follows that a controller designed to produce stable power-loop response at some short reactor period will produce more stable response at longer periods.

Figure 5 illustrates the effects of operating level on the open-power-loop response at an infinite reactor period. As shown, these effects are relatively minor and, consequently, should not influence the choice of controller to an extent as great as the reactor period does.

The power-loop responses (shown in figs. 4 and 5) begin to decrease at 25 radians per second, the natural frequency of the control-drum actuators. The addition of a type I controller (one containing a single $1/s$ term), therefore, would require only a

single lead term to maintain this bandwidth. The choice of control configuration, however, must take into account the period effects of the reactor. Table II illustrates the period effects at level I for three controller configurations that seemed promising on review of the loop characteristics. The configurations are

$$G_1(s) = \frac{K_c \left(1 + \dfrac{s}{10}\right)}{s \left(1 + \dfrac{s}{100}\right)}$$

$$G_2(s) = \frac{K_c \left(1 + \dfrac{s}{10}\right)^2}{s \left(1 + \dfrac{s}{100}\right)^2}$$

$$G_3(s) = \frac{K_c \left[1 + \dfrac{s}{25} + \left(\dfrac{s}{25}\right)^2\right]}{s \left(1 + \dfrac{s}{100}\right)^2}$$

The controller gain for each case was chosen to give a phase margin of 0° at a 0.5-second reactor period, thus ensuring positive phase margin for all periods greater than 0.5 second. This margin was assumed adequate, since under normal operating conditions this period should never be reached.

A large reduction in open-loop bandwidth occurred at infinite periods for each controller. This reduction was not as drastic with the use of the controller configuration $G_3(s)$. An additional advantage of this controller is that its use makes the analysis independent of the linear actuator dynamics, by essentially cancelling them. Therefore, $G_3(s)$ was picked as the power-loop controller.

Control-Loop Stability

The stability of the power control loop is indicated in table III. This table is a compilation of properties taken from Bode plots and root-locus diagrams of the open power loop $\Delta \log(Q_m/Q_o)/\Delta \log(Q_e/Q_o)$ at the operating levels and reactor periods under consideration. A 75-percent drop in bandwidth is apparent between 0.5-second and infinite periods, while the damping ratio increases from 0 to 1. These facts further evidence the

necessity of allowing marginal stability at a 0.5-second reactor period. Because of the large decrease in dynamic gain with increasing reactor period, a moderately wide bandwidth response at an infinite period is obtainable only under this condition.

The dependence of the power-loop stability on operating level is not nearly as striking, just as predicted in the preceding discussion. Whereas a difference of 75° or more separates the phase margin at an infinite period from that at a 0.5-second period, the separation between the phase margins at any two operating levels is less than 10°.

Closed-Loop Results

The closed-power-loop transfer functions with this controller are listed in table IV for infinite and 2-second reactor periods at the four operating levels. These transfer functions were derived from root-locus diagrams, which solved the general characteristic equation of

$$G_p = \frac{\Delta Q}{\Delta \log \dfrac{Q_d}{Q_o}} = \frac{G_{c,p} G_D G_r}{1 + G_{c,p} G_D G_r K_s}$$

Transfer functions for the 0.5-second period are not included because of the marginal stability characteristics of the system under this condition. Frequency-response plots corresponding to these transfer functions multiplied by K_s are presented in figure 6 for an infinite reactor period and in figure 7 for a 2-second reactor period. The increase in the bandwidth and magnitude of the resonant peak with decreased reactor period is evident on comparison of these figures. Each figure also indicates the almost negligible effects of operating level on the loop response of $\Delta \log(Q_m/Q_o)/\Delta \log(Q_d/Q_o)$. The response of $\Delta Q/\Delta \log(Q_d/Q_o)$ is, of course, extremely level dependent as far as the transfer-function gain is concerned (see table IV).

A verification of the linear analysis was accomplished by using

$$G_{c,p}(s) = \frac{385\left[1 + \dfrac{s}{25} + \left(\dfrac{s}{25}\right)^2\right]}{s\left(1 + \dfrac{s}{100}\right)^2}$$

as the power controller in the nonlinear analog simulation of the system. The closed-loop response of the simulation for small-amplitude disturbances is plotted for an infinite

reactor period in figure 6, and compares favorably with the analytically derived curve. The response at a 2-second reactor period was not made since a 2-second period implies a dynamic state of the simulation, which could not be evaluated readily in terms of frequency response.

CHAMBER-TEMPERATURE CONTROL UTILIZING AN INNER-POWER LOOP

System Description

The block diagram of the temperature control loop with an inner-power loop is presented in figure 8. The loop consists of a temperature controller acting on a temperature error signal to generate a log-power demand for the power control loop described in figure 8. The resulting change in power acts through the heat-transfer and flow system to vary the chamber temperature T. The other input to the heat-transfer and flow system, θ_v, is fixed at each operating level.

Chamber temperature is sensed by a thermocouple governed by the relation

$$G_{th} = \frac{\Delta T_m}{\Delta T} = \frac{1}{1 + \left(\frac{2.5}{\dot{w}}\right)s}$$

where $\dot{w}$ is the weight flow through the reactor core (ref. 6).

Open-Loop Dynamics

The dynamics of the open temperature loop, excluding controller dynamics, may be expressed in transfer-function form as

$$\frac{\Delta T_{m'}}{\Delta \log Q_d}\bigg|_{\theta_v} = G_p G_{s,t} G_{th} G_{th,m'}$$

This transfer function exhibits dependency both on operating level and reactor period. The values of G_p are those derived for the closed power loop and are given in table IV. Values for $G_{s,t}$ and G_{th} are given in table V for the four levels under consideration. The last term in the expression for the open-temperature-loop transfer function is a compensation for the thermocouple. Because of the large time constant of the thermocouple, the first step in developing a temperature control would be to apply a compensa-

10

tion network to the thermocouple, thereby extending its response. The compensation

$$G_{th, m'}(s) = \frac{1 + \dfrac{s}{3}}{1 + \dfrac{s}{60}}$$

was chosen since it gave approximate cancellation of the thermocouple lag over the power range of operation.

The reactor period effects on the open temperature loop are presented in figure 9. As shown, these effects are slight, resulting from the action of the power control loop as evidenced from the closed-loop response curves of figures 6 and 7. A comparison of these curves indicates negligible period effects up to a frequency of 10 radians per second. If the temperature-loop bandwidth is made less than this value, period effects may be neglected in the choice of a temperature controller.

Figure 10 illustrates the effect of operating level on the open-temperature-loop response. The contribution of the low-frequency pair of complex poles in the transfer function $G_{s, t} = \Delta T / \Delta Q$ (table V) is apparent in the sharp drop in magnitude and the excessive dip in phase angle below 1 radian per second. This dip in phase angle is especially apparent at levels III and IV. Therefore, in order to obtain adequate open-loop phase margin, at least one low-frequency zero must be present in a type I controller configuration.

Since there is more phase shift at levels III and IV than at level I, a comparison of controller configurations was made at level III. The open-loop response of the temperature loop $\Delta T_{m'} / \Delta T_e$, with the following controllers, is given in figure 11:

$$G_{1, i}(s) = \frac{K_c \left(1 + \dfrac{s}{\omega_i}\right)}{s\left(1 + \dfrac{s}{60}\right)}$$

where $\omega_1 = 1$, $\omega_2 = 0.5$, $\omega_3 = 0.1$, and $i = 1, 2, 3$.

$$G_2(s) = \frac{K_c \left(1 + \dfrac{s}{0.1}\right)\left(1 + \dfrac{s}{10}\right)}{s\left(1 + \dfrac{s}{60}\right)\left(1 + \dfrac{s}{100}\right)}$$

These configurations were picked as promising on review of the open-loop characteristics and pole-zero locations. Excessive dip in the phase-angle response is apparent with controller $G_{1, 1}$ and $G_{1, 2}$. The response of the loop with $G_{1, 3}$ is much improved.

The additional lead term of $G_2(s)$ further improves the phase-angle response of the loop, permitting wider open-loop bandwidths. However, bandwidths greater than 10 radians per second would not only increase the effects of reactor period on the loop but possibly might overdrive the power loop by causing excessively large demand perturbations. Therefore,

$$G_{c,t}(s) = \frac{K_c \left(1 + \dfrac{s}{0.1}\right)}{s\left(1 + \dfrac{s}{60}\right)}$$

was chosen as the temperature controller. It will produce a phase margin in excess of 40° at level III (at all bandwidths less than 6.8 rad/sec) with increased phase margin at the other levels under consideration, implying that the increased complexity of controllers of the type $G_2(s)$ is unwarranted.

Control-Loop Stability

A compilation of the stability characteristics of the loop with $G_{c,t}(s)$ as the controller is given in table VI for two different values of K_c. The first gain, $K_c = 6.5\times10^{-4}$, was picked to give a phase margin of approximately 50° and a dominant pole-damping ratio of 0.5 at level I and an infinite reactor period. The phase margins at the other levels for this gain were about the same as that at level I, but the open-loop bandwidths were decreased by approximately one-third. The second gain, $K_c = 2\times10^{-3}$, was picked to give a phase margin of approximately 46° and a damping ratio of 0.5 at level II and an infinite reactor period. Although the phase margins at levels II, III, and IV are still about the same with the broader bandwidth response, only a small phase margin exists at level I.

In order to obtain maximum bandwidths and stability at all levels, it is necessary to use an adaptive-gain controller. For this type of control, a function is needed to relate the controller gain to the system operating conditions. In this case, the controller gain must be a function of the operating level. Although the use of adaptive gain in this type of temperature control was not investigated, certain observations concerning its use may be made from table VI. Seemingly, the stability properties of the system at levels II and IV are similar for a constant controller gain, which could imply that chamber pressure might be useful in relating gain to operating level, since levels II and IV are at essentially constant pressure. A comparison of the stability properties at levels I, II, and III (at constant gain) indicates an inverse functional relation between the bandwidth

and chamber pressure. The adaptive principle was applied to the other method of temperature control, and the results are discussed in the subsequent section.

Closed-Loop Results

Closed-loop transfer functions were derived from root-locus diagrams used to solve the general characteristic equation

$$G_t = \frac{\Delta T}{\Delta T_d} = \frac{G_{c,t} G_p G_{s,t}}{1 + G_{c,t} G_p G_{s,t} G_{th} G_{th,m'}}$$

These transfer functions are listed in table VII for infinite and 2-second reactor periods at the four operating levels under consideration. Figures 12 and 13 show the frequency response of the system at infinite and 2-second reactor periods, respectively.

At an infinite reactor period (fig. 12), the 3db point (the frequency at which the response is 70.7 percent of its low frequency value) ranges from 0.37 hertz at level III to 2 hertz at level I. Figure 13 illustrates about the same characteristics for the response at a 2-second reactor period, indicating only slight effects of reactor period on the closed-temperature-loop response.

For verification of the analytical results, the controllers $G_{c,p}$ and $G_{c,t}$ were used to control the nonlinear analog simulation of the engine (ref. 2). The closed-loop frequency response was determined at the operating levels under consideration and at the conditions near infinite reactor period. The results are plotted on the analytically derived response curves of figure 12. No attempt was made to obtain simulation data for a 2-second reactor period for reasons given previously.

The correlation between the simulation data and the analytical data may be used as an indication of the accuracy of the use of the linear analysis in the evaluation of the nonlinear problem. Figure 12 indicates satisfactory results.

After the development of a pressure-control system, closed-temperature-loop data were taken at constant pressure demand rather than at constant turbine-power-control valve angle. No significant change in the closed-loop response was noticed. Therefore, the effect of a controlled chamber pressure on the open power and/or temperature loops is small, and open-loop transfer functions derived at constant turbine-power-control valve angle adequately describe the open-power-loop and temperature-loop dynamics.

CHAMBER TEMPERATURE CONTROL WITHOUT AN INNER-POWER LOOP

System Description

The block diagram of the temperature control loop without reactor power control is shown in figure 14. Transfer functions for $G_D(s)$ and $G_r(s)$ are listed in table I and those for $G_{s,t}(s)$ and $G_{th}(s)$ in table V. Elimination of the power loop provides direct manipulation of the control-drum actuators by the temperature controller. The resulting change in reactivity due to the drums is coupled with the inherent reactivity feedback to produce a change in reactor power. The transfer functions, relating the chamber temperature to reactor power, used in the analysis of this loop were again those derived at constant turbine-power-control valve angle. As with the other method of temperature control, the thermocouple (which is the same) was compensated by the transfer function

$$G_{th,m'}(s) = \frac{1 + \dfrac{s}{3}}{1 + \dfrac{s}{60}}$$

Open-Loop Dynamics

Open-loop dynamics, excluding controller dynamics, are given by the transfer function

$$\left.\frac{\Delta T_{m'}}{\Delta \theta_{D,d}}\right|_{\theta_v} = G_D G_r G_{s,t} G_{th} G_{th,m'}$$

Figure 15 illustrates the effects of the reactor period on the open-loop response, and figure 16 illustrates the effects of operating level on the open-loop response. These figures indicate that not only must the controller for this loop be able to handle a wide range of system dynamics between operating levels but it must also be able to handle the considerably large change in dynamics with reactor period. Figure 15 suggests the necessity of allowing only for marginal stability at a 0.5-second reactor period (as was done in the power control loop) in order to obtain moderately wide bandwidths at an infinite period. Figure 16 suggests the use of adaptive-gain control to account for the effects of operating level.

The choice of controller configuration was made by observing the phase margin and open-loop bandwidth characteristics of the system at levels I and III and at infinite and

0.5-second reactor periods for controllers of the types

$$G_1(s) = \frac{K_c(1 + s)}{s\left(1 + \dfrac{s}{60}\right)}$$

$$G_2(s) = \frac{K_c\left(1 + \dfrac{s}{0.1}\right)}{s\left(1 + \dfrac{s}{60}\right)}$$

$$G_3(s) = \frac{K_c\left(1 + \dfrac{s}{0.1}\right)\left(1 + \dfrac{s}{10}\right)}{s\left(1 + \dfrac{s}{60}\right)\left(1 + \dfrac{s}{100}\right)}$$

These controllers were picked as promising on review of the open-loop characteristics and pole-zero locations. The controller gain K_c used to compare the configurations was that gain for each configuration which would produce a phase margin of 0° at a 0.5-second period at level I.

The results (listed in table VIII) indicate that $G_1(s)$ allows a phase margin of only 9° at level III and at an infinite reactor period because of the low-frequency complex poles in the temperature to power transfer function. Little difference in phase margin or open-loop bandwidth can be noticed between the use of $G_2(s)$ or $G_3(s)$ as system controllers. Therefore, because of its relative simplicity, $G_2(s)$ was picked as the controller configuration for this loop.

Control-Loop Stability

Compared in table IX are the stability characteristics and the bandwidths of the temperature loop at the various conditions of operating level and reactor period. The response is considered for three controller gains. The controller gain $K_c = 7.5 \times 10^{-3}$ was chosen to produce a phase margin of 0° at level I and at a 0.5-second reactor period. Again, the decreasing bandwidth with increasing period is apparent at each operating level. The bandwidths at an infinite period range from 3.15 radians per second at level I to 0.86 radians per second at level III. The corresponding bandwidths at a 0.5-second period are much larger, ranging from 15.2 to 3.9 radians per second. This drop of approximately 80 percent in bandwidth in going from a 0.5-second period to an infinite

15

period evidences the need for allowing only marginal stability at a 0.5-second period, if moderately wide bandwidths at an infinite period are desired.

Although the marginal stability at a 0.5-second period at level I is not common to the other levels, the bandwidths at these levels are much narrower. It is apparent (as it was in controlling the chamber temperature with an inner-power loop) that the bandwidth at any level has a direct dependence on chamber pressure: level I, which has the highest chamber pressure, also has the broadest bandwidth; levels II and III, which have almost equal chamber pressures, have almost equivalent bandwidths; level III, which has the lowest chamber pressure of the levels considered, also has the narrowest bandwidth.

Since an increase in open-loop gain corresponds to an increase in open-loop bandwidth, it would be of value to schedule this gain as a function of chamber pressure so that a lower pressure would cause a higher controller gain. This scheduling would permit wider bandwidth response at the levels of lower chamber pressure. The problem of finding a function that would optimize the loop at every operating level could be formidable. As an approximation, the following linear relation between controller gain K_c and chamber pressure P was used:

$$K_c = -4.6 \times 10^{-5} P + 3.28 \times 10^{-2}$$

This function was picked to give a gain of $K_c = 7.5 \times 10^{-3}$ at level I and also to give a gain of $K_c = 2.13 \times 10^{-2}$ at level II, both of which produce conditions of marginal stability at their respective levels. The corresponding gains at levels III and IV are $K_c = 2.5 \times 10^{-2}$ and $K_c = 2.13 \times 10^{-2}$, respectively. As indicated in table IX, this function, although certainly not optimum, did generally double the bandwidth at levels II, III, and IV while it preserved phase margins of over 45° at these levels for reactor periods of 2 seconds or greater.

Closed-Loop Results

Closed-loop transfer functions were derived from root-locus diagrams used to solve the general characteristic equation

$$G_t = \frac{\Delta T}{\Delta T_d} = \frac{G_{c,t} G_D G_r G_{s,t}}{1 + G_{c,t} G_D G_r G_{s,t} G_{th} G_{th,m'}}$$

These transfer functions are given in table X for infinite and 2-second reactor periods at the four operating levels and for the various controller gains discussed in the previous section. Figures 17 and 18 give the frequency response of the system at infinite and

16

2-second reactor periods, respectively, corresponding to the transfer functions for the fixed-gain case $K_c = 7.5 \times 10^{-3}$.

The effect of reactor period on the closed-temperature-loop response is evident from a comparison of figure 17 with figure 18. In general, larger resonant peaks and an increased bandwidth characterize a movement to shorter reactor periods, which is as predicted in table IX.

Figure 17 indicates that for the fixed-gain case, the 3db point at level I is at 0.5 hertz; at levels II and IV, 0.32 hertz; and at level III, 0.21 hertz (better than a 2 to 1 change over the considered operating range). A similar spread is apparent in figure 18 for a 2-second period.

Figure 19 illustrates the closed-temperature-loop response at infinite reactor period when adaptive-gain control is used. The controller gain was determined according to the relation

$$K_c = -4.6 \times 10^{-5} P + 3.28 \times 10^{-2}$$

Comparison of figure 19 with figure 17 reveals a marked increase in the closed-loop bandwidth at levels II, III, and IV over that obtained with a fixed K_c. A smaller dependency of response on operating level is evidenced by the greater similarity of the frequency response at the various levels, especially at levels I, II, and IV. The facts that the response at level III does not seem to match that at the other levels and that there is a large amount of peaking at level IV indicate that the linear relation between K_c and P is not precisely the function which will eliminate operating-level effects from the loop response. It does, however, diminish the effects to a useful extent.

The fixed gain controller, as well as the adaptive-gain controller, were used to control the analog simulation of the engine. The closed-loop frequency response was then determined at the various operating levels for an infinite reactor period. The results are plotted in figure 17 for the fixed-gain case and in figure 19 for the case in which adaptive-gain control was used. The close agreement of these data with the analytically derived curves lends verification to the linear analysis.

CHAMBER-PRESSURE CONTROL

System Description

A block diagram of the pressure control loop is presented in figure 20. The controller accepts a pressure error signal and converts it to a turbine-power-control valve

angle demand $\theta_{v,d}$ as input to the valve actuators. They are assumed linear and have the transfer function

$$G_v(s) = \frac{1}{1 + \dfrac{s}{62.8} + \left(\dfrac{s}{62.8}\right)^2}$$

The resulting turbine-power-control valve angle θ_v is an input to the heat-transfer and flow system.

In the development of this analysis, in a combination chamber-temperature chamber-pressure control system, accurate description of the chamber pressure (P) to turbine-power-control valve (θ_v) transfer function can be made only if the temperature control loop is closed. System analysis made at constant control-drum position will not be valid because of the effect of temperature variations on the open-pressure-loop gain. A comparison of the $\Delta P/\Delta\theta_v$ transfer functions for constant control-drum position and constant temperature demand is given in table XI. The pressure sensor is assumed to have a gain of 1 and negligible dynamics.

Open-Loop Dynamics

The dynamics of the open pressure loop, excluding controller dynamics, are expressed in transfer-function form as

$$\left.\frac{\Delta P}{\Delta\theta_{v,d}}\right|_{T_d} = G_v G_{s,p}$$

This transfer function is dependent on operating level, as shown in table XI and in the Bode plots of $\Delta P/\Delta\theta_{v,d}$ in figure 21. This transfer function is also dependent on reactor period because of the effects of θ_v on the inherent reactivity feedback. It was assumed, for purposes of analytic simplification, that this dependency is negligible. There is some justification for this assumption. Since the chamber-pressure response can be affected only by the dynamics of the reactivity loop through changes in reactor power and corresponding changes in chamber temperature, the period dependency is greatly diminished by closure of the control loops around the power and/or chamber temperature. This effect on reactor period can be seen by a comparison of figures 17 and 18 which present the frequency-response plots of the closed temperature loop at infinite and 2-second reactor periods, respectively.

18

The dead time present in the system transfer functions (table XI) is evident in the plots of the phase angle in figure 21. Because of this sharp drop in phase angle and the initial first-order drop in magnitude, little advantage can be gained by using more than a first-order lead in a type I pressure controller.

The effects of operating level on the response of the system are primarily manifested in the magnitude plots of figure 21. Little effect of operating level on phase angle is apparent. Therefore, the choice of controller configuration can be made by observing the characteristics of various controllers at levels II and IV, which form the boundaries of the magnitude plot. The phase and gain margins at these levels are given in table XII for controllers of the type

$$G_i(s) = \frac{K_c\left(1 + \dfrac{s}{\omega_i}\right)}{s\left(1 + \dfrac{s}{100}\right)}$$

where $\omega_1 = 0.5$, $\omega_2 = 1$, $\omega_3 = 5$, and $i = 1, 2, 3$.

The choice of controller configuration was made by observing the open-loop characteristics of the system. Because of the presence of the dead time, an increase in phase margin by the addition of lead terms in the controller configuration is deterred at frequencies greater than about 25 radians per second (see fig. 21). The open-loop pole-zero locations indicate that a single lead-lag term should be sufficient to extend the bandwidths to this frequency.

The gain of each controller transfer function was picked to give a minimum phase margin of 40° at level IV. This level was picked as the yardstick since it is the level of maximum gain (fig. 21) and of nearly minimum phase angle. Controllers with $\omega = 0.5$ and 1 show practically identical characteristics. An $\omega = 5$ produces a slightly better open-loop bandwidth and gain margin at the two levels. Although there is a reduction in phase margin at level II, using this controller, it is still adequate. The pressure-loop controller was therefore chosen to be

$$G_{c,pr}(s) = \frac{1.43\left(1 + \dfrac{s}{5}\right)}{s\left(1 + \dfrac{s}{100}\right)}$$

Control-Loop Stability

The stability properties of the pressure loop, with the aforementioned controller at

the four operating levels, were obtained from open-loop Bode plots and root-locus diagrams and are presented in table XIII. The response ranges from being overdamped at level III to underdamped at level IV. System stability seems to decrease with increasing temperature at constant pressure from level II to IV and seems to increase with increasing pressure at constant temperature from level IV to I.

The sensitivity of the pressure-loop bandwidth is also indicated in table XIII. Decreasing the pressure from level I to level IV and from level II to level III is accompanied by an increase in bandwidth. Decreasing the temperature from level IV to level II is accompanied by a sharp decrease in bandwidth.

Closed-Loop Results

Closed-pressure-loop transfer functions were derived from root-locus plots used to solve the general characteristic equation

$$G_{pr} = \frac{\Delta P}{\Delta P_d} = \frac{G_{c,pr}G_v G_{s,p}}{1 + G_{c,pr}G_v G_{s,p}}$$

These transfer functions are listed in table XIV. The closed-loop response was plotted from these transfer functions and is presented in figure 22. The response is quite level dependent with 3db points ranging in frequency from 0.78 hertz at level II to 6.8 hertz at level IV. The peaking at level IV is also quite formidable, indicating that perhaps at some conditions of low chamber pressure and high chamber temperature, the loop would become unstable.

The controller $G_{c,pr}$ was used to control the nonlinear analog simulation. The closed-loop frequency response of the simulation at the four levels under consideration is plotted in figure 22. More discrepancy exists between the analytical and simulation data in this loop than in the other control loops. This discrepancy may be attributed to greater nonlinearities in the pressure loop, which did not permit accurate representation of the transfer function $G_{s,pr} = \Delta P/\Delta \theta_v$.

Although there is quite a variation in the response of the pressure loop to changes in operating level, no investigation of the use of adaptive control in this loop was made. A more thorough investigation of the open-loop characteristics must be made before the necessary functional relations between gain and operating level can be determined.

POWER-RANGE STARTUPS

From an individual analysis of each control loop, controllers for reactor power, chamber pressure, and two types of chamber temperature control were developed for use in the power range of engine operation.

A block diagram illustrating the use of a power loop in the control of the engine is shown in figure 23. Transfer functions for the controller and compensation networks, developed in the previous sections, are given in this diagram.

The ability of this type of engine control system to handle power-range startups was tested by using simultaneous linear startup demands in chamber temperature and pressure. Figure 24 illustrates the transient response of the engine simulation to demand ramps of 100° R per second in temperature and 15.8 pounds per square inch per second in pressure. The system was ramped from a steady-state condition at 100 pounds per square inch and 1250° R to the design level of 550 pounds per square inch and 4090° R.

The initial peak temperature error was about 68° R with an overall average error of approximately 40° R. The initial error in the pressure loop was about 4.8 pounds per square inch with an average error of less than 1.3 pounds per square inch. Increasing loop bandwidth as the system approaches the design level accounts for the gradual decrease in error magnitude in both loops.

Overshoot in reactor power due to the action of the temperature controller is apparent. The average value of δk is about 31 cents. Through the use of material available in reference 1, this value may be related to an average reactor period of about 17 seconds.

Figure 25 illustrates the transient response of this system to a ramp rate of 150° R per second in temperature and 23.8 pounds per square inch per second in pressure. Temperature error increased to a peak of about 87° R and an average of approximately 60° R. Pressure error increased correspondingly. The average δk increased to about 40 cents, indicating an average reactor period of approximately 9 seconds.

Control of the engine simulation without the use of a power control loop is diagramed in figure 26. Transfer functions for the controller and compensation networks are given. Startups using this control technique, with constant temperature controller gain $K_c = 7.5 \times 10^{-3}$, are given in figures 27 and 28. Again, the startups were made from steady-state conditions at 100 pounds per square inch and 1250° R to the design level.

Ramp rates of 100° R per second and 15.8 pounds per square inch per second (fig. 27) produce an initial error of 98° R in the temperature loop and an average error of about 70° R.

The initial error in the pressure loop is about 5 pounds per square inch with an average of about 1.3 pounds per square inch. As discussed previously, this error in the pressure loop is not appreciably influenced by the choice of the temperature control tech-

nique. The average value of δk is about 30 cents, indicating an average reactor period of about 16.5 seconds.

Figure 28 illustrates the transient response of the fixed-gain system to a ramp rate of 150° R per second in temperature and 23.8 pounds per square inch per second in pressure. The temperature error increased to a peak of about 120° R and an average of about 100° R. The pressure error increased correspondingly. The average δk increased to about 36 cents, indicating an average reactor period of approximately 12 seconds.

The use of adaptive-gain control in the temperature loop is illustrated by the dashed line in figure 26. The temperature loop gain is made a linear function of pressure demand. This function $K_c = -4.6 \times 10^{-5} P_d + 3.28 \times 10^{-2}$, was determined in a preceding section (p. 16).

The transient response of the adaptive system is shown in figure 29. The system was ramped from the steady-state condition at 100 pounds per square inch and 1250° R to the design level with a ramp of 100° R per second in temperature and 15.8 pounds per square inch per second in pressure. This is a startup comparable to the response made with fixed-controller gains (see fig. 27).

The initial peak temperature error, obtained by using variable temperature controller gain, was only 35° R with an average error of approximately the same. The initial peak pressure error was 2.75 pounds per square inch with an average error only slightly above zero. The large reduction in error at low operating levels, from that when fixed controller gains were used, is due to the increased low-level bandwidth of the temperature loop. The error at design level is not reduced since both the adaptive- and fixed-gain controllers have the same gain at this level.

When the loop response was increased, the adaptive system did not increase the average δk. The reactor period and the average δk are approximately what they were during the startup when the fixed controller gain was used.

CONCLUDING REMARKS

The results of this investigation indicate that linear analysis techniques can be used to develop controllers for a NERVA-type nuclear rocket engine (as described in ref. 2) which will be stable over a wide range of operating conditions. Wide-bandwidth response at all operating conditions is not possible with linear controllers because of the large variations in engine dynamics with operating level and reactor period.

Adaptive-gain control may be used to compensate somewhat for the operating level effects. Linear analysis can be useful in obtaining functional relations between the controller gain and system variables for use with an adaptive controller.

The investigation also indicates that only a small advantage is gained in system dynamics with the use of an inner-power loop to control the chamber temperature. The use of an inner-power loop does allow slightly better temperature-loop bandwidth by partly eliminating the restrictions imposed on the gain of the temperature controller by the effects of reactor period. However, there are other reasons, not considered in this investigation, for including an inner-power loop. For safety, fast-reactor transients can be sensed quicker by more direct neutron flux or power level measurements than they can by thermal measurements. Control action can then be taken before parameters reach destructive levels. A second reason for including an inner-power loop is that closed-loop control of the reactor can be maintained at relatively low power levels where insufficient thermal power may be measured or where temperature-loop stability may be questionable.

CONCLUSIONS

From an analysis of the controls of a nuclear rocket engine at power range operating conditions, several specific conclusions have been reached:

Power Control

The effects of operating level on the open-loop dynamics are negligible compared with the effects of reactor period.

The controller transfer function

$$G_{c,p}(s) = \frac{385\left[1 + \dfrac{s}{25} + \left(\dfrac{s}{25}\right)^2\right]}{s\left(1 + \dfrac{s}{100}\right)^2}$$

will allow stable operation of the control loop at the four operating levels investigated and at reactor periods as low as 0.5-second. At all investigated operating conditions, bandwidths greater than 1 hertz are obtainable.

Temperature-Power Control

The effects of reactor period on the open-loop dynamics are minimized because of the presence of the inner-power loop. Operating level, however, has a large effect on the open-loop dynamics. The filter $(1 + s/3)/(1 + s/60)$ will produce compensation for the thermocouple over the power range of operation and will permit loop bandwidths of greater than 1 hertz at level I with the controller

$$G_{c,t}(s) = \frac{6.5\times10^{-4}\left(1 + \dfrac{s}{0.1}\right)}{s\left(1 + \dfrac{s}{60}\right)}$$

The bandwidth decreases, however, at the lower operating levels. At level III, the bandwidth with this controller is 0.4 hertz. This bandwidth may be increased by increasing the controller gain. A gain of 2×10^{-3} allows stable operation at level III with a bandwidth of 0.9 hertz.

Temperature Control Without Power Control

The open-loop dynamics exhibit a large dependence on both operating level and reactor period.

When the thermocouple compensation network $(1 + s/3)/(1 + s/60)$ is used, the controller transfer function

$$G_{c,t}(s) = \frac{7.5\times10^{-3}\left(1 + \dfrac{s}{0.1}\right)}{s\left(1 + \dfrac{s}{60}\right)}$$

will allow stable operation of the engine at all operating levels investigated and at reactor periods as low as 0.5 second. The maximum bandwidth, which occurs at level I, is only slightly greater than 0.5 hertz for an infinite reactor period. The minimum bandwidth occurs at level III and is slightly greater than 0.2 hertz.

Stable operation with increased bandwidths at levels II, III, and IV may be obtained by scheduling controller gain as a function of chamber pressure. The use of the function $K_c = -4.6\times10^{-5} P + 3.28\times10^{-2}$ yields the following bandwidths at infinite reactor periods: level I, 0.5 hertz; level II, 0.6 hertz; level III, 0.45 hertz; and level IV, 0.7 hertz.

Pressure Control

The open loop dynamics can be considered as independent of reactor period effects if the chamber temperature is under closed-loop control.

Although the open-loop dynamics exhibit a rather strong dependence on operating level, stable wide-bandwidth response (approx. 1 Hz) is obtainable over the power range of operation with the controller

$$G_{c, pr}(s) = \frac{1.43\left(1 + \dfrac{s}{5}\right)}{s\left(1 + \dfrac{s}{100}\right)}$$

Control-Loop Interaction

The effect of a controlled chamber pressure on the open power and/or temperature loops is small. Transfer functions, relating the controlled to the manipulated variables in these loops and obtained at fixed turbine-power-control-valve angle, are adequate to predict the open-loop dynamics.

The dynamics of the open pressure loop are altered by the closure of the temperature loop. A comparison of the open-loop transfer function taken at constant temperature demand to that taken at constant control-drum reactivity reveals a general decrease in transfer function gain as well as an extension in the break frequency of the dominant pole.

Power Range Startups

Power range startups of 100° and 150° R per second produce average temperature-loop errors of 30° and 40° R higher, respectively, without the use of a power loop than with it.

The use of an adaptive-gain controller in the temperature loop without an inner-power loop reduces by one-half the average error during a startup transient.

While increasing the temperature-loop response, the adaptive controller does not noticeably increase the load on the reactor kinetics. The average δk and reactor period are approximately what they were during comparable startups with a fixed-controller gain.

Lewis Research Center,
    National Aeronautics and Space Administration,
        Cleveland, Ohio, January 30, 1967,
            122-29-03-06-22.

REFERENCES

1. Hearn, Thomas O.: NRDS Analysis of the KIWI B-4D-202 Nuclear Reactor Control System. Rep. No. LA-3301-MS, Los Alamos Scientific Lab., Sept. 20, 1965.

2. Hart, Clint E.; and Arpasi, Dale J.: Frequency Response and Transfer Functions of a Nuclear Rocket Engine System Obtained From Analog Computer Simulation. NASA TN D-3979, 1967.

3. Singer, Sidney: The Period Equilibrium Effect in Reactor Dynamics. Rep. No. LA-2654, Los Alamos Scientific Lab., Jan. 1962.

4. Morgan, M. L.; and Looney, J. C.: Design of the ESIAC Algebraic Computer. IRE Trans. on Electronic Computers, vol. EC-10, no. 3, Sept. 1961, pp. 524-529.

5. Morgan, M. L.: The Construction and Use of Logarithmic Pole-Zero Root Locus and Frequency Response Plots. Paper No. 2.2.63, Instrument Society of America, Sept. 9-12, 1963.

6. Anon.: AGC-WANL Common Model for Analog Computer. Report No. RN-S-0240, Aerojet-General Corporation, July 1965.

TABLE I. - POWER-CONTROL-LOOP TRANSFER FUNCTIONS

Operating level	Reactor power sensor, $K_s(l)$, sec/Btu	Actuators and drum worth, $G_D(s, l)$, reactivity/deg	Reactor period, τ, sec	Reactivity loop at constant turbine-power-control valve, $G_r(s, l, \tau)$, Btu/(sec reactivity)
I	4.072×10^{-7}	$\dfrac{5.92\times10^{-4}}{1 + \frac{s}{25} + \left(\frac{s}{25}\right)^2}$	∞	$\dfrac{7.14\times10^7 \left(1 + \frac{s}{0.0276}\right)\left(1 + \frac{s}{0.235}\right)\left(1 + \frac{s}{0.48}\right)\left(1 + \frac{s}{1.65}\right)}{\left(1 + \frac{s}{0.0241}\right)\left(1 + \frac{s}{0.204}\right)\left[1 + \frac{1.86s}{1.45} + \left(\frac{s}{1.45}\right)^2\right]\left(1 + \frac{s}{312}\right)}$
			2	$\dfrac{7.14\times10^7 \left(1 + \frac{s}{0.48}\right)\left(1 + \frac{s}{0.735}\right)\left(1 + \frac{s}{2.15}\right)\left(1 + \frac{s}{71}\right)}{\left(1 + \frac{s}{0.82}\right)\left[1 + \frac{1.68s}{2.45} + \left(\frac{s}{2.45}\right)^2\right]\left(1 + \frac{s}{62}\right)\left(1 + \frac{s}{105}\right)}$
			0.5	$\dfrac{7.14\times10^7 \left(1 + \frac{s}{0.48}\right)\left(1 + \frac{s}{2.24}\right)\left(1 + \frac{s}{3.65}\right)\left(1 + \frac{s}{71}\right)}{\left(1 + \frac{s}{2.53}\right)\left[1 + \frac{1.5s}{4.7} + \left(\frac{s}{4.7}\right)^2\right]\left(1 + \frac{s}{30.24}\right)\left(1 + \frac{s}{81.24}\right)}$
II	1.335×10^{-6}	$\dfrac{5.92\times10^{-4}}{1 + \frac{s}{25} + \left(\frac{s}{25}\right)^2}$	∞	$\dfrac{4.76\times10^7 \left(1 + \frac{s}{0.0276}\right)\left(1 + \frac{s}{0.235}\right)\left(1 + \frac{s}{0.7}\right)\left(1 + \frac{s}{1.65}\right)}{\left(1 + \frac{s}{0.0208}\right)\left(1 + \frac{s}{0.17}\right)\left[1 + \frac{1.88s}{1.4} + \left(\frac{s}{1.4}\right)^2\right]\left(1 + \frac{s}{312}\right)}$
			2	$\dfrac{4.76\times10^7 \left(1 + \frac{s}{0.7}\right)\left(1 + \frac{s}{2.15}\right)\left(1 + \frac{s}{68}\right)^2}{\left[1 + \frac{1.82s}{2.1} + \left(\frac{s}{2.1}\right)^2\right]\left(1 + \frac{s}{51}\right)\left(1 + \frac{s}{83}\right)\left(1 + \frac{s}{101.5}\right)}$
			0.5	$\dfrac{4.76\times10^7 \left(1 + \frac{s}{0.7}\right)\left(1 + \frac{s}{2.24}\right)\left(1 + \frac{s}{3.65}\right)\left(1 + \frac{s}{68}\right)^2}{\left(1 + \frac{s}{2.58}\right)\left[1 + \frac{1.34s}{4.0} + \left(\frac{s}{4.0}\right)^2\right]\left(1 + \frac{s}{25.5}\right)\left[1 + \frac{1.96s}{79} + \left(\frac{s}{79}\right)^2\right]}$
III	2.047×10^{-6}	$\dfrac{5.99\times10^{-4}}{1 + \frac{s}{25} + \left(\frac{s}{25}\right)^2}$	∞	$\dfrac{2.94\times10^7 \left(1 + \frac{s}{0.0276}\right)\left(1 + \frac{s}{0.235}\right)\left(1 + \frac{s}{0.4}\right)\left(1 + \frac{s}{1.65}\right)}{\left(1 + \frac{s}{0.0212}\right)\left(1 + \frac{s}{0.184}\right)\left(1 + \frac{s}{0.82}\right)\left(1 + \frac{s}{1.24}\right)\left(1 + \frac{s}{312}\right)}$
			2	$\dfrac{2.94\times10^7 \left(1 + \frac{s}{0.4}\right)\left(1 + \frac{s}{0.735}\right)\left(1 + \frac{s}{2.15}\right)\left(1 + \frac{s}{73}\right)^2}{\left(1 + \frac{s}{1.05}\right)\left[1 + \frac{1.5s}{1.35} + \left(\frac{s}{1.35}\right)^2\right]\left(1 + \frac{s}{55}\right)\left(1 + \frac{s}{84}\right)\left(1 + \frac{s}{101.5}\right)}$
			0.5	$\dfrac{2.94\times10^7 \left(1 + \frac{s}{0.4}\right)\left(1 + \frac{s}{2.24}\right)\left(1 + \frac{s}{3.65}\right)\left(1 + \frac{s}{73}\right)^2}{\left(1 + \frac{s}{2.55}\right)\left[1 + \frac{s}{2.9} + \left(\frac{s}{2.9}\right)^2\right]\left(1 + \frac{s}{34}\right)\left[1 + \frac{1.96s}{79} + \left(\frac{s}{79}\right)^2\right]}$
IV	9.083×10^{-7}	$\dfrac{5.6\times10^{-4}}{1 + \frac{s}{25} + \left(\frac{s}{25}\right)^2}$	∞	$\dfrac{3.06\times10^7 \left(1 + \frac{s}{0.0276}\right)\left(1 + \frac{s}{0.2}\right)\left(1 + \frac{s}{0.235}\right)\left(1 + \frac{s}{1.65}\right)}{\left(1 + \frac{s}{0.0246}\right)\left(1 + \frac{s}{0.255}\right)\left(1 + \frac{s}{0.535}\right)\left(1 + \frac{s}{1.28}\right)\left(1 + \frac{s}{312}\right)}$
			2	$\dfrac{3.06\times10^7 \left(1 + \frac{s}{0.2}\right)\left(1 + \frac{s}{0.735}\right)\left(1 + \frac{s}{2.15}\right)}{\left(1 + \frac{s}{1.15}\right)\left[1 + \frac{1.41s}{1.33} + \left(\frac{s}{1.33}\right)^2\right]\left(1 + \frac{s}{101.5}\right)}$
			0.5	$\dfrac{3.06\times10^7 \left(1 + \frac{s}{0.2}\right)\left(1 + \frac{s}{2.24}\right)\left(1 + \frac{s}{3.65}\right)}{\left(1 + \frac{s}{2.76}\right)\left[1 + \frac{s}{3} + \left(\frac{s}{3}\right)^2\right]\left(1 + \frac{s}{41}\right)}$

TABLE II. - OPEN-LOOP COMPARISON OF CONTROLLER CONFIGURATIONS FOR

POWER-LOOP CONTROL AT LEVEL I

Controller configuration, $\Delta\theta_{D,d}\big/\big[\Delta \log(Q_e/Q_o)\big]$, deg	Controller gain, K_c	Reactor period, τ, sec					
		0.5			∞		
		Open-loop bandwidth, rad/sec	Phase margin, deg	Gain margin, dB	Open-loop bandwidth, rad/sec	Phase margin, deg	Gain margin, dB
$G_1(s) = \dfrac{K_c\left(1 + \dfrac{s}{10}\right)}{s\left(1 + \dfrac{s}{100}\right)}$	84.7	30.5	0	0	3.1	106	21.6
$G_2(s) = \dfrac{K_c\left(1 + \dfrac{s}{10}\right)^2}{s\left(1 + \dfrac{s}{100}\right)^2}$	71.9	50.0	0	0	2.8	120	21.2
$G_3(s) = \dfrac{K_c\left[1 + \dfrac{s}{25} + \left(\dfrac{s}{25}\right)^2\right]}{s\left(1 + \dfrac{s}{100}\right)^2}$	385	41.0	0	0	12.3	77	22.2

TABLE III. - STABILITY PROPERTIES OF POWER CONTROL LOOP

$$G_{c,p}(s) = \frac{385\left[1 + \dfrac{s}{25} + \left(\dfrac{s}{25}\right)^2\right]}{s\left(1 + \dfrac{s}{100}\right)^2}.$$

Power controller, $G_{c,p}(s) = $

Operating level	Reactor period, τ, sec											
	0.5				2				∞			
	Open-loop bandwidth, rad/sec	Phase margin, deg	Gain margin, dB	Damping ratio	Open-loop bandwidth, rad/sec	Phase margin, deg	Gain margin, dB	Damping ratio	Open-loop bandwidth, rad/sec	Phase margin, deg	Gain margin, dB	Damping ratio
I	41	0	0	0	31	45	9	0.33	12.3	77	22.2	1.0
II	42	0	0	0	30.5	46	10	0.31	11.6	79	23	1.0
III	43.5	1	0.2	0	32	40	8.6	0.33	12.7	75	21.2	1.0
IV	41	4	1	0.05	28.5	47	9.6	0.37	9.9	78	24	1.0

TABLE IV. - CLOSED-POWER-LOOP TRANSFER FUNCTIONS

$$\left[\text{Power controller, } G_{c,p}(s) = \frac{385\left[1 + \frac{s}{25} + \left(\frac{s}{25}\right)^2\right]}{s\left(1 + \frac{s}{100}\right)^2}\right.$$

Operating level	Reactor period, τ, sec	Closed-power-loop transfer function, $G_p(s, l, \tau) = \Delta Q \big/ \left[\Delta \log(Q_d/Q_o)\right]$, Btu/sec
I	∞	$\dfrac{2.456\times10^6}{\left(1 + \frac{s}{27}\right)\left(1 + \frac{s}{37}\right)\left(1 + \frac{s}{150}\right)\left(1 + \frac{s}{312}\right)}$
	2	$\dfrac{2.45\times10^6\left(1 + \frac{s}{71}\right)}{\left[1 + \frac{0.65\,s}{45} + \left(\frac{s}{45}\right)^2\right]\left(1 + \frac{s}{85}\right)\left[1 + \frac{1.86\,s}{152} + \left(\frac{s}{152}\right)^2\right]}$
II	∞	$\dfrac{7.488\times10^5}{\left(1 + \frac{s}{22}\right)\left(1 + \frac{s}{41}\right)\left(1 + \frac{s}{150}\right)\left(1 + \frac{s}{312}\right)}$
	2	$\dfrac{7.488\times10^5}{\left[1 + \frac{0.62\,s}{44} + \left(\frac{s}{44}\right)^2\right]\left[1 + \frac{1.86\,s}{150} + \left(\frac{s}{150}\right)^2\right]}$
III	∞	$\dfrac{4.886\times10^5}{\left(1 + \frac{s}{21.5}\right)\left(1 + \frac{s}{40}\right)\left(1 + \frac{s}{150}\right)\left(1 + \frac{s}{312}\right)}$
	2	$\dfrac{4.886\times10^5}{\left[1 + \frac{0.65\,s}{42} + \left(\frac{s}{42}\right)^2\right]\left[1 + \frac{1.86\,s}{148} + \left(\frac{s}{148}\right)^2\right]}$
IV	∞	$\dfrac{1.1\times10^6}{\left(1 + \frac{s}{14.8}\right)\left(1 + \frac{s}{49}\right)\left(1 + \frac{s}{146}\right)\left(1 + \frac{s}{312}\right)}$
	2	$\dfrac{1.1\times10^6}{\left[1 + \frac{0.74\,s}{43} + \left(\frac{s}{43}\right)^2\right]\left[1 + \frac{1.82\,s}{150} + \left(\frac{s}{150}\right)^2\right]}$

TABLE V. - TEMPERATURE-LOOP TRANSFER FUNCTIONS

Operating level	Thermocouple, $G_{th}(s, l)$	Ratio of temperature- to power-transfer function at constant turbine-power-control valve, $G_{s,t}(s, l)$, $^{\circ}R\text{-sec/Btu}$
I	$\dfrac{1}{1 + \dfrac{s}{3.4}}$	$\dfrac{2.6\times10^{-3}\left(1 + \dfrac{s}{1.55}\right)}{\left[1 + \dfrac{1.41\,s}{0.5} + \left(\dfrac{s}{0.5}\right)^2\right]\left(1 + \dfrac{s}{90}\right)}$
II	$\dfrac{1}{1 + \dfrac{s}{2.8}}$	$\dfrac{3.7\times10^{-3}\left(1 + \dfrac{s}{1.55}\right)}{\left[1 + \dfrac{1.41\,s}{0.45} + \left(\dfrac{s}{0.45}\right)^2\right]\left(1 + \dfrac{s}{90}\right)}$
III	$\dfrac{1}{1 + \dfrac{s}{2.24}}$	$\dfrac{6.75\times10^{-3}\left(1 + \dfrac{s}{1.25}\right)}{\left[1 + \dfrac{1.41\,s}{0.27} + \left(\dfrac{s}{0.27}\right)^2\right]\left(1 + \dfrac{s}{90}\right)}$
IV	$\dfrac{1}{1 + \dfrac{s}{2.28}}$	$\dfrac{6.0\times10^{-3}\left(1 + \dfrac{s}{1.2}\right)}{\left[1 + \dfrac{1.41\,s}{0.26} + \left(\dfrac{s}{0.26}\right)^2\right]\left(1 + \dfrac{s}{90}\right)}$

TABLE VI. - STABILITY PROPERTIES OF TEMPERATURE CONTROL LOOP

WITH INNER-POWER LOOP

$$\left[\text{Power controller, } G_{c,p}(s) = \frac{385\left[1 + \frac{s}{25} + \left(\frac{s}{25}\right)^2\right]}{s\left(1 + \frac{s}{100}\right)^2} \text{ and temperature controller, } G_{c,t}(s) = \frac{K_c\left(1 + \frac{s}{0.1}\right)}{s\left(1 + \frac{s}{60}\right)}.\right]$$

Controller gain, K_c	Operating level	Reactor period, τ, sec							
		2				∞			
		Open-loop bandwidth, rad/sec	Phase margin, deg	Gain margin, dB	Damping ratio	Open-loop bandwidth, rad/sec	Phase margin, deg	Gain margin, dB	Damping ratio
6.5×10^{-4}	I	6.5	67	12.6	0.72	6.1	54	11.8	0.5
	II	2.6	64	22.6	0.71	2.5	55	21.2	0.71
	III	1.38	42	32.1	0.42	1.48	44	28.3	0.5
	IV	2.3	52	20.9	0.54	2.3	48	19.1	0.59
2×10^{-3}	I	18.8	27	2.8	(a)	13.8	11	2	(a)
	II	6.3	63	12.8	0.77	6	46	11.4	0.5
	III	2.75	51	22.3	0.6	3.1	48	18.5	0.67
	IV	6	56	11.1	0.93	5.5	38	9.3	0.5

[a]Not determined.

TABLE VII. - CLOSED-TEMPERATURE-LOOP TRANSFER FUNCTIONS

$$\left[\text{Power controller, } G_{c,p}(s) = \frac{385}{s}\,\frac{\left[1 + \dfrac{s}{25} + \left(\dfrac{s}{25}\right)^2\right]}{\left(1 + \dfrac{s}{100}\right)^2} \text{ and temperature controller, } G_{c,t}(s) = \frac{K_c\left(1 + \dfrac{s}{0.1}\right)}{s\left(1 + \dfrac{s}{60}\right)}\right]$$

Controller gain, K_c	Operating level	Reactor period, τ, sec	Closed-temperature-loop transfer functions, $G_t(s, l, \tau) = \Delta T/\Delta T_d$
6.5×10^{-4}	I	∞	$\dfrac{\left(1 + \frac{s}{1.55}\right)\left(1 + \frac{s}{3.4}\right)\left(1 + \frac{s}{60}\right)}{\left(1 + \frac{s}{2.25}\right)\left(1 + \frac{s}{2.5}\right)\left[1 + \frac{s}{10.5} + \left(\frac{s}{10.5}\right)^2\right]\left[1 + \frac{1.66s}{53} + \left(\frac{s}{53}\right)^2\right]\left[1 + \frac{1.98s}{88} + \left(\frac{s}{88}\right)^2\right]\left(1 + \frac{s}{150}\right)\left(1 + \frac{s}{312}\right)}$
		2	$\dfrac{\left(1 + \frac{s}{1.55}\right)\left(1 + \frac{s}{3.4}\right)\left(1 + \frac{s}{60}\right)}{\left(1 + \frac{s}{2.45}\right)\left[1 + \frac{1.44s}{19} + \left(\frac{s}{19}\right)^2\right]\left[1 + \frac{0.65s}{45} + \left(\frac{s}{45}\right)^2\right]\left(1 + \frac{s}{71}\right)\left[1 + \frac{1.28s}{100} + \left(\frac{s}{100}\right)^2\right]\left[1 + \frac{1.86s}{152} + \left(\frac{s}{152}\right)^2\right]}$
	II	∞	$\dfrac{\left(1 + \frac{s}{1.55}\right)\left(1 + \frac{s}{60}\right)}{\left[1 + \frac{1.41s}{2.25} + \left(\frac{s}{2.25}\right)^2\right]\left(1 + \frac{s}{11.5}\right)\left[1 + \frac{1.88s}{50} + \left(\frac{s}{50}\right)^2\right]\left[1 + \frac{1.98s}{90} + \left(\frac{s}{90}\right)^2\right]\left(1 + \frac{s}{150}\right)\left(1 + \frac{s}{312}\right)}$
		2	$\dfrac{\left(1 + \frac{s}{1.55}\right)\left(1 + \frac{s}{60}\right)}{\left[1 + \frac{1.41s}{2.1} + \left(\frac{s}{2.1}\right)^2\right]\left(1 + \frac{s}{35}\right)\left[1 + \frac{0.62s}{44} + \left(\frac{s}{44}\right)^2\right]\left(1 + \frac{s}{73}\right)\left(1 + \frac{s}{78}\right)\left[1 + \frac{1.86s}{150} + \left(\frac{s}{150}\right)^2\right]}$
	III	∞	$\dfrac{\left(1 + \frac{s}{1.25}\right)\left(1 + \frac{s}{2.24}\right)\left(1 + \frac{s}{60}\right)}{\left[1 + \frac{s}{1.38} + \left(\frac{s}{1.38}\right)^2\right]\left(1 + \frac{s}{1.95}\right)\left(1 + \frac{s}{16.5}\right)\left[1 + \frac{1.94s}{49} + \left(\frac{s}{49}\right)^2\right]\left(1 + \frac{s}{78}\right)\left(1 + \frac{s}{90}\right)\left(1 + \frac{s}{150}\right)\left(1 + \frac{s}{312}\right)}$
		2	$\dfrac{\left(1 + \frac{s}{1.25}\right)\left(1 + \frac{s}{2.24}\right)}{\left[1 + \frac{0.84s}{1.35} + \left(\frac{s}{1.35}\right)^2\right]\left(1 + \frac{s}{2.05}\right)\left[1 + \frac{0.65s}{42} + \left(\frac{s}{42}\right)^2\right]\left(1 + \frac{s}{46}\right)\left(1 + \frac{s}{90}\right)\left[1 + \frac{1.86s}{148} + \left(\frac{s}{148}\right)^2\right]}$
	IV	∞	$\dfrac{\left(1 + \frac{s}{1.2}\right)\left(1 + \frac{s}{2.28}\right)\left(1 + \frac{s}{60}\right)}{\left(1 + \frac{s}{1.6}\right)\left[1 + \frac{1.18s}{2.2} + \left(\frac{s}{2.2}\right)^2\right]\left(1 + \frac{s}{11}\right)\left[1 + \frac{1.91s}{51} + \left(\frac{s}{51}\right)^2\right]\left(1 + \frac{s}{77}\right)\left(1 + \frac{s}{90}\right)\left(1 + \frac{s}{146}\right)\left(1 + \frac{s}{312}\right)}$
		2	$\dfrac{\left(1 + \frac{s}{1.2}\right)\left(1 + \frac{s}{2.28}\right)\left(1 + \frac{s}{60}\right)}{\left(1 + \frac{s}{1.65}\right)\left[1 + \frac{1.28s}{2} + \left(\frac{s}{2}\right)^2\right]\left[1 + \frac{0.75s}{43} + \left(\frac{s}{43}\right)^2\right]\left(1 + \frac{s}{44}\right)\left(1 + \frac{s}{78}\right)\left(1 + \frac{s}{90}\right)\left[1 + \frac{1.82s}{150} + \left(\frac{s}{150}\right)^2\right]}$

TABLE VIII. - OPEN-LOOP COMPARISON OF CONTROLLER CONFIGURATIONS FOR

TEMPERATURE-LOOP CONTROL AT LEVELS I AND III

Control configuration, $\Delta\theta_{dr,d}/\Delta T_e$ deg/$^{\circ}$R	Controller gain, K_c	Operating level	Reactor period, τ, sec					
			0.5			∞		
			Open-loop bandwidth, rad/sec	Phase margin, deg	Gain margin, dB	Open-loop bandwidth, rad/sec	Phase margin, deg	Gain margin, dB
$G_1(s) = \dfrac{K_c(1+s)}{s\left(1+\dfrac{s}{60}\right)}$	7.14×10^{-2}	I	15.2	0	0	2.9	63	17.8
		III	3.85	47	16.5	1.04	9	35
$G_2(s) = \dfrac{K_c\left(1+\dfrac{s}{0.1}\right)}{s\left(1+\dfrac{s}{60}\right)}$	7.5×10^{-3}	I	15.2	0	0	3.15	78	17
		III	3.9	59	16.5	0.86	51	34
$G_3(s) = \dfrac{K_c\left(1+\dfrac{s}{0.1}\right)\left(1+\dfrac{s}{10}\right)}{s\left(1+\dfrac{s}{60}\right)\left(1+\dfrac{s}{100}\right)}$	5.78×10^{-3}	I	22.2	0	0	2.55	90	17.2
		III	3.5	83	18.2	0.74	57	34

TABLE IX. - STABILITY PROPERTIES OF TEMPERATURE-CONTROL LOOP WITHOUT INNER-POWER LOOP

$$\left[\text{Temperature controller, } G_{c,t}(s) = \frac{K_c\left(1 + \dfrac{s}{0.1}\right)}{s\left(1 + \dfrac{s}{60}\right)}.\right]$$

Controller gain, K_c	Operating level	Reactor period, τ, sec											
		0.5				2				∞			
		Open-loop bandwidth, rad/sec	Phase angle, deg	Gain margin, dB	Damping ratio	Open-loop bandwidth, rad/sec	Phase angle, deg	Gain margin, dB	Damping ratio	Open-loop bandwidth, rad/sec	Phase angle, deg	Gain margin, dB	Damping ratio
7.5×10^{-3}	I	15.2	0	0	0	8.3	56	7	0.29	3.15	78	17	0.5
	II	6.6	62	9	(a)	2.75	82	17.5	0.64	1.28	68	27.3	0.5
	III	3.9	59	16.5	(a)	2.05	63.0	23.8	0.47	0.86	51	34	0.5
	IV	7.0	47	6.9	(a)	3.22	55	16.2	0.5	1.18	53	28.5	0.5
2.13×10^{-2}	I	26.0	-87	-9	(b)	19.5	-17.0	-2	(b)	7.7	60	8	(a)
	II	14.2	0	0	(a)	7.0	58	8.5	0.39	2.75	67	18.3	0.5
2.5×10^{-2}	III	7.9	29	6.6	(a)	4.75	51	13.3	0.62	1.88	48	23.5	0.5
2.13×10^{-2}	IV	17.2	-23	-2.1	(b)	7.1	46	7.2	0.64	2.33	53	19.5	0.5

[a]Not determined.
[b]Negative.

TABLE X. - CLOSED-TEMPERATURE-LOOP TRANSFER FUNCTIONS

$$\left[\text{Temperature controller, } G_{c,t}(s) = \frac{K_c\left(1 + \dfrac{s}{0.1}\right)}{s\left(1 + \dfrac{s}{60}\right)}.\right]$$

Controller gain, K_c	Operating level	Reactor period, τ, sec	Closed-temperature-loop transfer functions, $G_t(s, l, \tau) = \Delta T / \Delta T_d$
7.5×10^{-3}	I	∞	$$\frac{\left(1 + \frac{s}{0.48}\right)\left(1 + \frac{s}{1.55}\right)\left(1 + \frac{s}{1.65}\right)\left(1 + \frac{s}{3.4}\right)\left(1 + \frac{s}{60}\right)}{\left(1 + \frac{s}{0.62}\right)\left(1 + \frac{s}{1.12}\right)\left[1 + \frac{1.76\,s}{2.3} + \left(\frac{s}{2.3}\right)^2\right]\left(1 + \frac{s}{4.5}\right)\left[1 + \frac{s}{25} + \left(\frac{s}{25}\right)^2\right]\left(1 + \frac{s}{48}\right)\left(1 + \frac{s}{72}\right)\left(1 + \frac{s}{90}\right)\left(1 + \frac{s}{312}\right)}$$
		2	$$\frac{\left(1 + \frac{s}{0.48}\right)\left(1 + \frac{s}{1.55}\right)\left(1 + \frac{s}{2.15}\right)\left(1 + \frac{s}{3.4}\right)\left(1 + \frac{s}{60}\right)\left(1 + \frac{s}{71}\right)}{\left(1 + \frac{s}{0.61}\right)\left(1 + \frac{s}{1.1}\right)\left[1 + \frac{1.98\,s}{2.8} + \left(\frac{s}{2.8}\right)^2\right]\left(1 + \frac{s}{4}\right)\left[1 + \frac{0.58\,s}{16} + \left(\frac{s}{16}\right)^2\right]\left(1 + \frac{s}{46}\right)\left[1 + \frac{1.94\,s}{78} + \left(\frac{s}{78}\right)^2\right]\left(1 + \frac{s}{81}\right)\left(1 + \frac{s}{105}\right)}$$
	II	∞	$$\frac{\left(1 + \frac{s}{0.7}\right)\left(1 + \frac{s}{1.55}\right)\left(1 + \frac{s}{1.65}\right)}{\left[1 + \frac{1.81\,s}{1.05} + \left(\frac{s}{1.05}\right)^2\right]\left[1 + \frac{1.48\,s}{1.42} + \left(\frac{s}{1.42}\right)^2\right]\left[1 + \frac{s}{25} + \left(\frac{s}{25}\right)^2\right]\left(1 + \frac{s}{60}\right)\left(1 + \frac{s}{90}\right)\left(1 + \frac{s}{312}\right)}$$
		2	$$\frac{\left(1 + \frac{s}{0.7}\right)\left(1 + \frac{s}{1.55}\right)\left(1 + \frac{s}{2.15}\right)\left(1 + \frac{s}{68}\right)^2}{\left[1 + \frac{1.91\,s}{0.94} + \left(\frac{s}{0.94}\right)^2\right]\left[1 + \frac{1.89\,s}{3.55} + \left(\frac{s}{3.55}\right)^2\right]\left[1 + \frac{1.28\,s}{22} + \left(\frac{s}{22}\right)^2\right]\left(1 + \frac{s}{30.5}\right)\left(1 + \frac{s}{60}\right)\left(1 + \frac{s}{87}\right)^2\left(1 + \frac{s}{101.5}\right)}$$
	III	∞	$$\frac{\left(1 + \frac{s}{0.4}\right)\left(1 + \frac{s}{2.24}\right)}{\left(1 + \frac{s}{0.55}\right)\left[1 + \frac{1.06\,s}{0.87} + \left(\frac{s}{0.87}\right)^2\right]\left[1 + \frac{s}{25} + \left(\frac{s}{25}\right)^2\right]\left(1 + \frac{s}{69}\right)\left(1 + \frac{s}{90}\right)\left(1 + \frac{s}{312}\right)}$$
		2	$$\frac{\left(1 + \frac{s}{0.4}\right)\left(1 + \frac{s}{0.735}\right)\left(1 + \frac{s}{1.25}\right)\left(1 + \frac{s}{2.15}\right)\left(1 + \frac{s}{73}\right)^2}{\left[1 + \frac{1.93\,s}{0.52} + \left(\frac{s}{0.52}\right)^2\right]\left(1 + \frac{s}{1.55}\right)\left[1 + \frac{0.94\,s}{2.1} + \left(\frac{s}{2.1}\right)^2\right]\left[1 + \frac{s}{25} + \left(\frac{s}{25}\right)^2\right]\left(1 + \frac{s}{55}\right)\left(1 + \frac{s}{60}\right)\left(1 + \frac{s}{87}\right)^2\left(1 + \frac{s}{101.5}\right)}$$
	IV	∞	$$\frac{\left(1 + \frac{s}{1.65}\right)}{\left[1 + \frac{s}{1.2} + \left(\frac{s}{1.2}\right)^2\right]\left[1 + \frac{s}{25} + \left(\frac{s}{25}\right)^2\right]\left(1 + \frac{s}{60}\right)\left(1 + \frac{s}{90}\right)\left(1 + \frac{s}{312}\right)}$$
		2	$$\frac{\left(1 + \frac{s}{0.2}\right)\left(1 + \frac{s}{0.735}\right)\left(1 + \frac{s}{2.15}\right)\left(1 + \frac{s}{60}\right)}{\left(1 + \frac{s}{0.225}\right)\left(1 + \frac{s}{0.64}\right)\left[1 + \frac{1.14\,s}{3} + \left(\frac{s}{3}\right)^2\right]\left[1 + \frac{s}{25} + \left(\frac{s}{25}\right)^2\right]\left(1 + \frac{s}{48}\right)\left(1 + \frac{s}{72}\right)\left(1 + \frac{s}{90}\right)\left(1 + \frac{s}{101.5}\right)}$$

TABLE X. - Concluded.   CLOSED-TEMPERATURE-LOOP TRANSFER FUNCTIONS

$$\left[\text{Temperature controller, } G_{c,t}(s) = \frac{K_c\left(1 + \dfrac{s}{0.1}\right)}{s\left(1 + \dfrac{s}{60}\right)}.\right]$$

Controller gain, K_c	Operating level	Reactor period, τ, sec	Closed-temperature-loop transfer functions, $G_t(s, l, \tau) = \Delta T/\Delta T_d$
2.13×10^{-2}	II	∞	$$\frac{\left(1+\frac{s}{0.7}\right)\left(1+\frac{s}{1.55}\right)\left(1+\frac{s}{1.65}\right)\left(1+\frac{s}{60}\right)}{\left(1+\frac{s}{0.92}\right)\left(1+\frac{s}{1.03}\right)\left[1+\frac{1.64\,s}{2.5}+\left(\frac{s}{2.5}\right)^2\right]\left[1+\frac{s}{25}+\left(\frac{s}{25}\right)^2\right]\left(1+\frac{s}{47}\right)\left(1+\frac{s}{73}\right)\left(1+\frac{s}{90}\right)\left(1+\frac{s}{312}\right)}$$
		2	$$\frac{\left(1+\frac{s}{0.7}\right)\left(1+\frac{s}{1.55}\right)\left(1+\frac{s}{2.15}\right)\left(1+\frac{s}{68}\right)^2}{\left(1+\frac{s}{0.84}\right)\left(1+\frac{s}{1.33}\right)\left(1+\frac{s}{2.7}\right)\left[1+\frac{0.78\,s}{15}+\left(\frac{s}{15}\right)^2\right]\left[1+\frac{1.74\,s}{32}+\left(\frac{s}{32}\right)^2\right]\left(1+\frac{s}{60}\right)\left(1+\frac{s}{87}\right)^2\left(1+\frac{s}{101.5}\right)}$$
2.5×10^{-2}	III	∞	$$\frac{\left(1+\frac{s}{0.4}\right)\left(1+\frac{s}{2.24}\right)}{\left(1+\frac{s}{0.46}\right)\left[1+\frac{1.14\,s}{1.73}+\left(\frac{s}{1.73}\right)^2\right]\left[1+\frac{s}{25}+\left(\frac{s}{25}\right)^2\right]\left(1+\frac{s}{72}\right)\left(1+\frac{s}{90}\right)\left(1+\frac{s}{312}\right)}$$
		2	$$\frac{\left(1+\frac{s}{0.4}\right)\left(1+\frac{s}{0.735}\right)\left(1+\frac{s}{1.25}\right)\left(1+\frac{s}{2.15}\right)\left(1+\frac{s}{73}\right)^2}{\left(1+\frac{s}{0.48}\right)\left(1+\frac{s}{0.62}\right)\left(1+\frac{s}{1.55}\right)\left[1+\frac{1.23\,s}{3.8}+\left(\frac{s}{3.8}\right)^2\right]\left[1+\frac{1.2\,s}{23}+\left(\frac{s}{23}\right)^2\right]\left(1+\frac{s}{35}\right)\left(1+\frac{s}{60}\right)\left(1+\frac{s}{87}\right)^2\left(1+\frac{s}{101.5}\right)}$$
2.13×10^{-2}	IV	∞	$$\frac{\left(1+\frac{s}{1.65}\right)\left(1+\frac{s}{60}\right)}{\left[1+\frac{1.15\,s}{2.1}+\left(\frac{s}{2.1}\right)^2\right]\left[1+\frac{s}{25}+\left(\frac{s}{25}\right)^2\right]\left(1+\frac{s}{50}\right)\left(1+\frac{s}{68}\right)\left(1+\frac{s}{90}\right)\left(1+\frac{s}{312}\right)}$$
		2	$$\frac{\left(1+\frac{s}{2.15}\right)\left(1+\frac{s}{60}\right)}{\left[1+\frac{1.9\,s}{7.2}+\left(\frac{s}{7.2}\right)^2\right]\left[1+\frac{1.31\,s}{18}+\left(\frac{s}{18}\right)^2\right]\left(1+\frac{s}{33}\right)\left[1+\frac{1.98\,s}{83}+\left(\frac{s}{83}\right)^2\right]\left(1+\frac{s}{101.5}\right)}$$

TABLE XI. - COMPARISON OF OPEN-PRESSURE-LOOP TRANSFER FUNCTIONS

WITH AND WITHOUT CLOSED-TEMPERATURE-LOOP CONTROL

Operating level	Pressure to turbine-power-control-valve angle transfer functions	
	With constant control-drum reactivity, $G_{s,pr}(s, l) = \dfrac{\Delta P_c}{\Delta \theta_v}\bigg|_{\delta k_D}$, psi/deg	With constant temperature demand, $G_{s,pr}(s, l) = \dfrac{\Delta P_c}{\Delta \theta_v}\bigg|_{T_d}$, psi/deg
I	$\dfrac{16.5\left(1 + \dfrac{s}{0.45}\right)e^{-0.02\,s}}{\left(1 + \dfrac{s}{0.29}\right)\left(1 + \dfrac{s}{5.3}\right)}$	$\dfrac{10.95\left(1 + \dfrac{s}{39}\right)e^{-0.02\,s}}{\left(1 + \dfrac{s}{4.8}\right)\left(1 + \dfrac{s}{49}\right)}$
II	$\dfrac{5.95\left(1 + \dfrac{s}{0.3}\right)e^{-0.024\,s}}{\left(1 + \dfrac{s}{0.18}\right)\left(1 + \dfrac{s}{3.2}\right)}$	$\dfrac{4.0\left(1 + \dfrac{s}{39}\right)e^{-0.027\,s}}{\left(1 + \dfrac{s}{2.8}\right)\left(1 + \dfrac{s}{49}\right)}$
III	$\dfrac{20.0\left(1 + \dfrac{s}{0.145}\right)e^{-0.035\,s}}{\left(1 + \dfrac{s}{0.09}\right)\left(1 + \dfrac{s}{2.5}\right)}$	$\dfrac{11.9\left(1 + \dfrac{s}{39}\right)e^{-0.03\,s}}{\left(1 + \dfrac{s}{1.95}\right)\left(1 + \dfrac{s}{49}\right)}$
IV	$\dfrac{35.0\left(1 + \dfrac{s}{0.17}\right)e^{-0.022\,s}}{\left(1 + \dfrac{s}{0.14}\right)\left(1 + \dfrac{s}{2.3}\right)}$	$\dfrac{30.5\left(1 + \dfrac{s}{39}\right)e^{-0.027\,s}}{\left(1 + \dfrac{s}{2.2}\right)\left(1 + \dfrac{s}{49}\right)}$

TABLE XII. - OPEN-LOOP COMPARISON OF CONTROLLER

CONFIGURATIONS FOR PRESSURE-LOOP CONTROL

Controller configuration, $\Delta\theta_{v,d}/\Delta P_e$, deg/psi	Controller gain, K_c	Operating level	Open-loop bandwidth, rad/sec	Phase margin, deg	Gain margin, dB
$G_1(s) = \dfrac{K_c\left(1 + \dfrac{s}{0.5}\right)}{s\left(1 + \dfrac{s}{100}\right)}$	1.8×10^{-1}	II	2.55	123	19
		IV	22	40	3.8
$G_2(s) = \dfrac{K_c(1 + s)}{s\left(1 + \dfrac{s}{100}\right)}$	3.37×10^{-1}	II	2.55	113	19.4
		IV	21.5	40	4
$G_3(s) = \dfrac{K_c\left(1 + \dfrac{s}{5}\right)}{s\left(1 + \dfrac{s}{100}\right)}$	1.43	II	4.1	64	23.7
		IV	17.5	40	5

TABLE XIII. - STABILITY PROPERTIES OF

PRESSURE-CONTROL LOOP

$$\left[\text{Pressure controller, } G_{c,pr}(s) = \frac{1.43\left(1 + \dfrac{s}{5}\right)}{s\left(1 + \dfrac{s}{100}\right)}\right]$$

Operating level	Open-loop bandwidth, rad/sec	Phase margin, deg	Gain margin, deg	Damping ratio
I	14.5	64	8	0.45
II	3.85	65	17	0.5
III	7.3	52	13.6	0.86
IV	18.5	40	4.5	0.29

TABLE XIV. - CLOSED-PRESSURE-LOOP TRANSFER FUNCTIONS

$$\left[\text{Pressure controller, } G_{c,\,pr}(s) \;=\; \frac{1.43\left(1 + \dfrac{s}{5}\right)}{s\left(1 + \dfrac{s}{100}\right)}\,.\right]$$

Operating level	Closed-pressure-loop transfer functions, $G_{p,\,r}(s) = \Delta P/\Delta P_D$
I	$$\dfrac{\left(1 + \dfrac{s}{39}\right)e^{-0.02\,s}}{\left(1 + \dfrac{s}{29}\right)\left[1 + \dfrac{0.91\,s}{36.5} + \left(\dfrac{s}{36.5}\right)^2\right]\left[1 + \dfrac{1.53\,s}{95} + \left(\dfrac{s}{95}\right)^2\right]}$$
II	$$\dfrac{\left(1 + \dfrac{s}{5}\right)\left(1 + \dfrac{s}{39}\right)e^{-0.027\,s}}{\left[1 + \dfrac{1.39\,s}{4.2} + \left(\dfrac{s}{4.2}\right)^2\right]\left[1 + \dfrac{1.94\,s}{61} + \left(\dfrac{s}{61}\right)^2\right]\left[1 + \dfrac{s}{62.8} + \left(\dfrac{s}{62.8}\right)^2\right]}$$
III	$$\dfrac{\left(1 + \dfrac{s}{5}\right)\left(1 + \dfrac{s}{39}\right)e^{-0.03\,s}}{\left[1 + \dfrac{1.41\,s}{6.8} + \left(\dfrac{s}{6.8}\right)^2\right]\left[1 + \dfrac{1.71\,s}{40} + \left(\dfrac{s}{40}\right)^2\right]\left[1 + \dfrac{1.18\,s}{83} + \left(\dfrac{s}{83}\right)^2\right]\left(1 + \dfrac{s}{200}\right)}$$
IV	$$\dfrac{\left(1 + \dfrac{s}{5}\right)\left(1 + \dfrac{s}{39}\right)e^{-0.027\,s}}{\left(1 + \dfrac{s}{6.6}\right)\left(1 + \dfrac{s}{37.5}\right)\left[1 + \dfrac{0.58\,s}{29} + \left(\dfrac{s}{29}\right)^2\right]\left[1 + \dfrac{1.18\,s}{99} + \left(\dfrac{s}{99}\right)^2\right]}$$
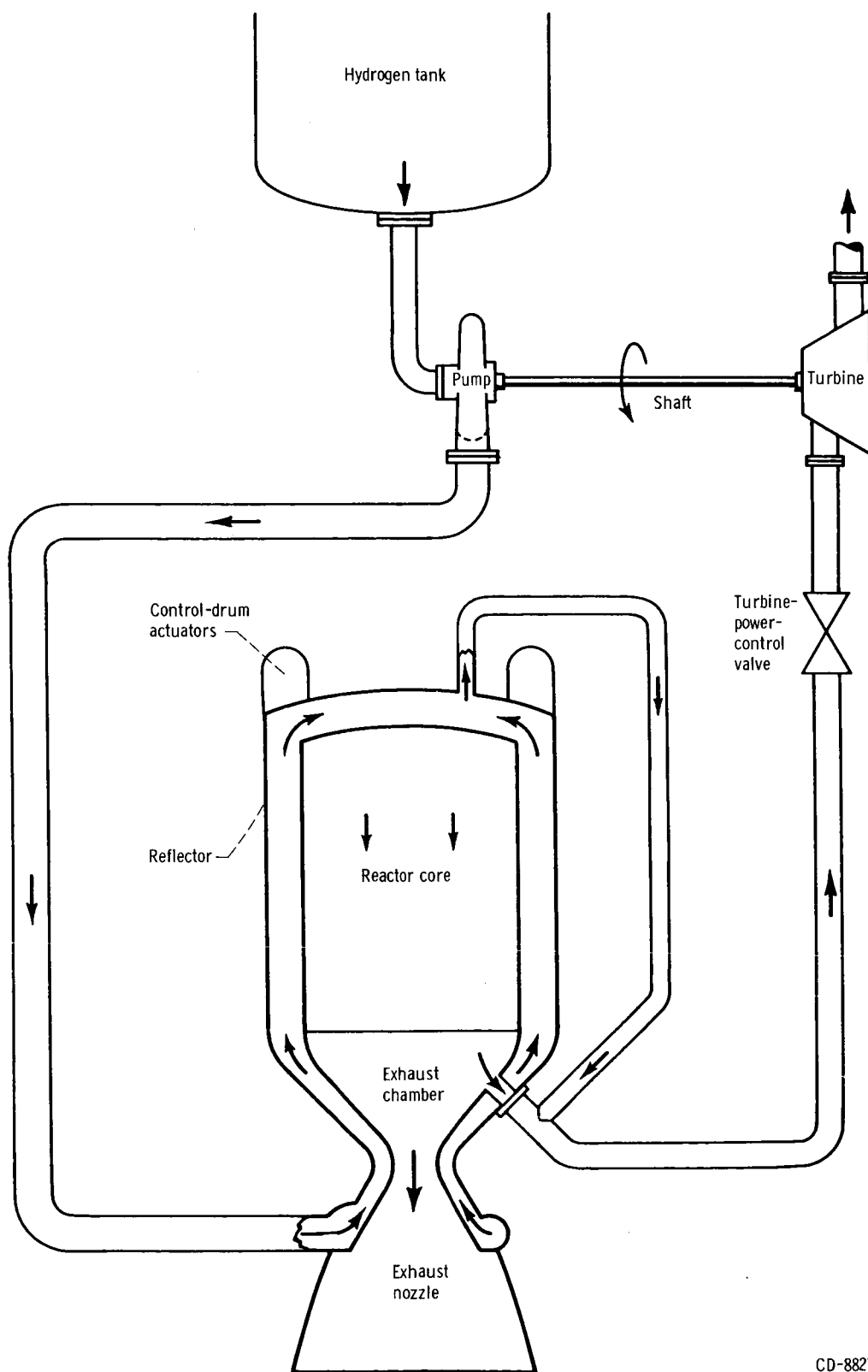
Figure 1. - Flow diagram of nuclear rocket engine.

CD-8827
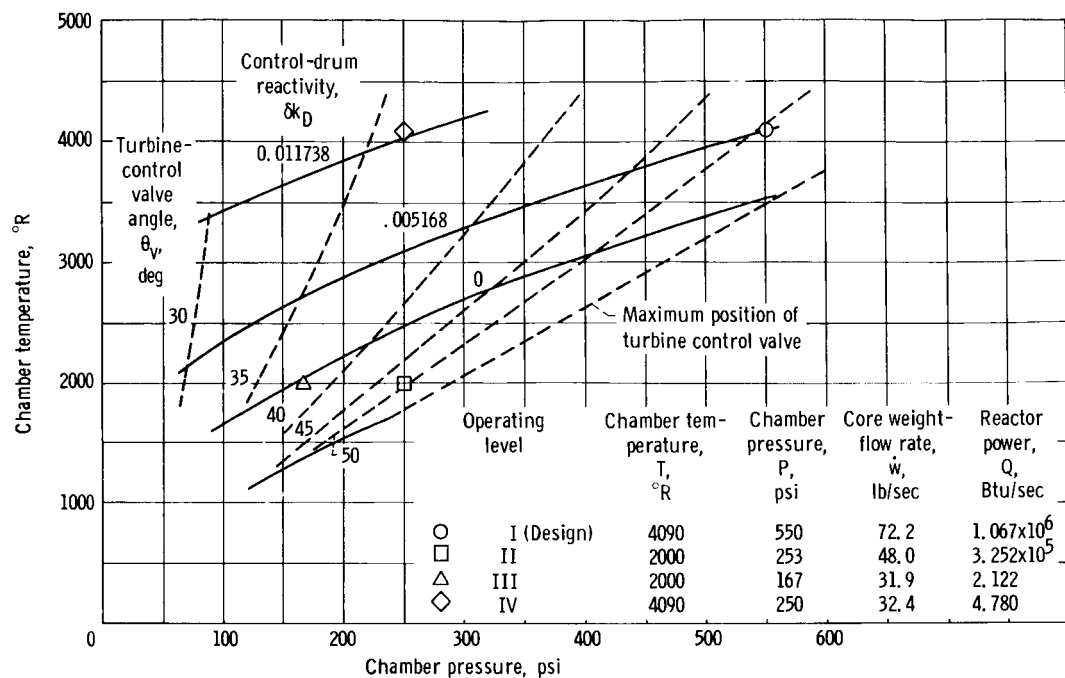
Figure 2. - Steady-state operating map over power range.

	Operating level	Chamber temperature, T, °R	Chamber pressure, P, psi	Core weight-flow rate, ẇ, lb/sec	Reactor power, Q, Btu/sec
O	I (Design)	4090	550	72.2	1.067×10^6
□	II	2000	253	48.0	3.252×10^5
△	III	2000	167	31.9	2.122
◇	IV	4090	250	32.4	4.780
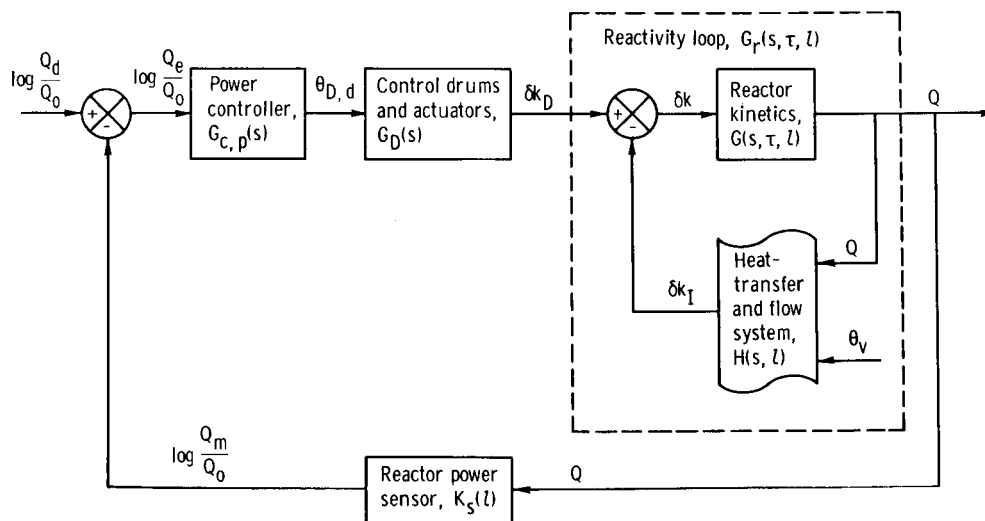
Figure 3. - Power control loop.

42
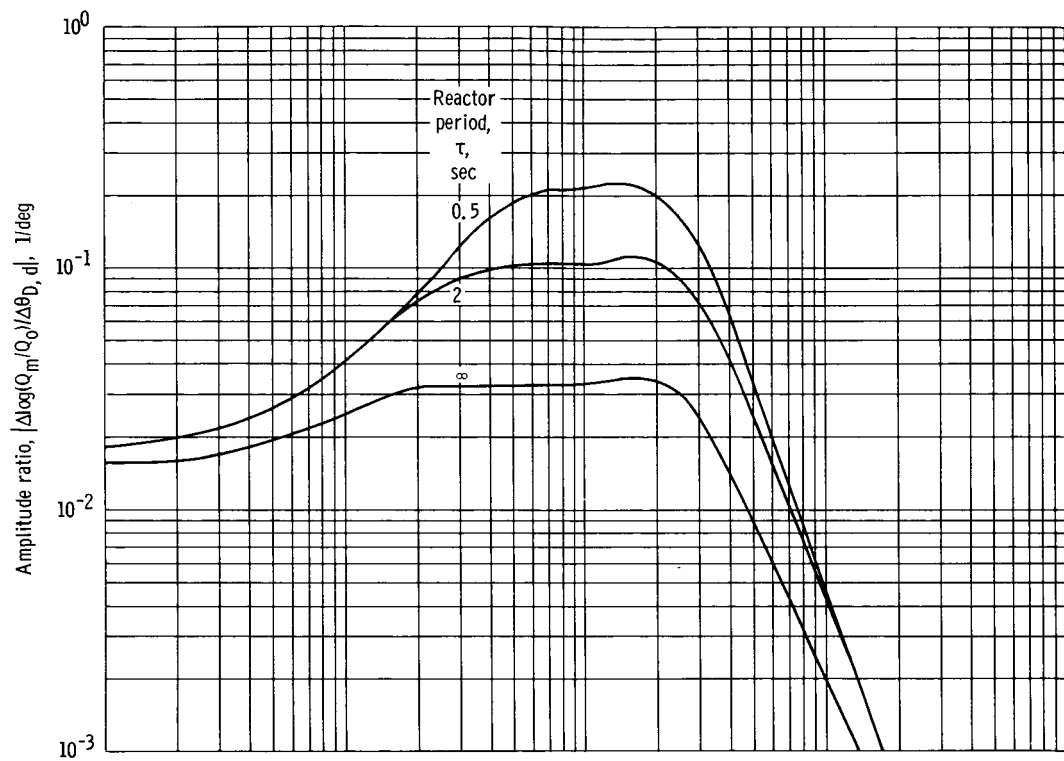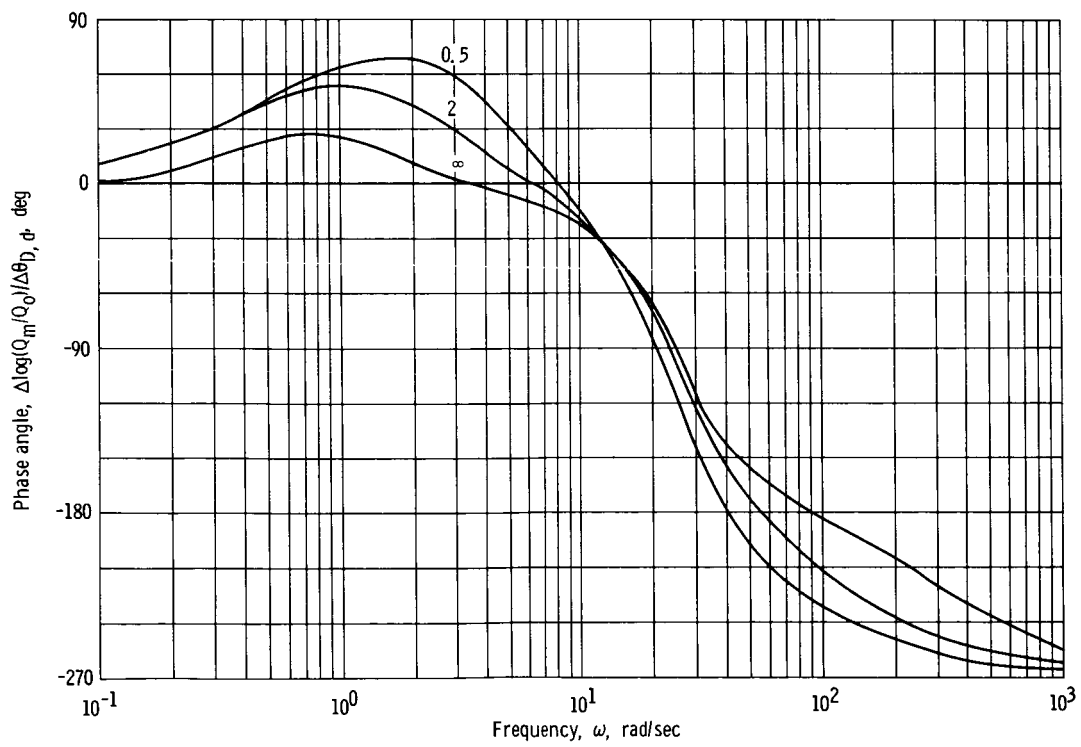
(a) Amplitude ratio.

(b) Phase angle.

Figure 4. – Reactor period effects on open power loop without controller compensation at level I.
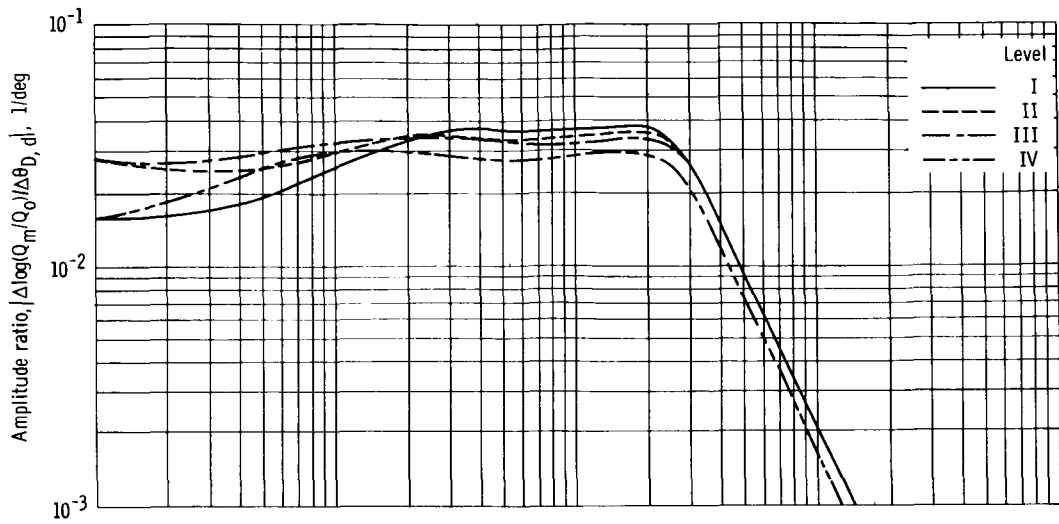
(a) Amplitude ratio.
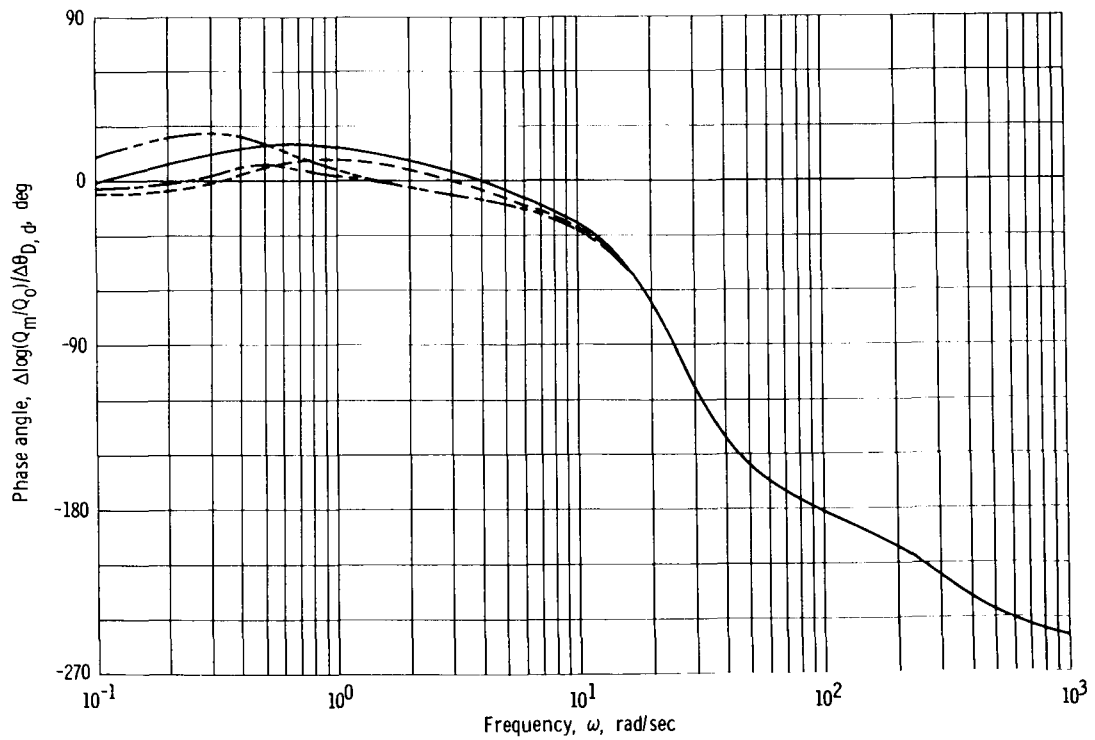
(b) Phase angle.

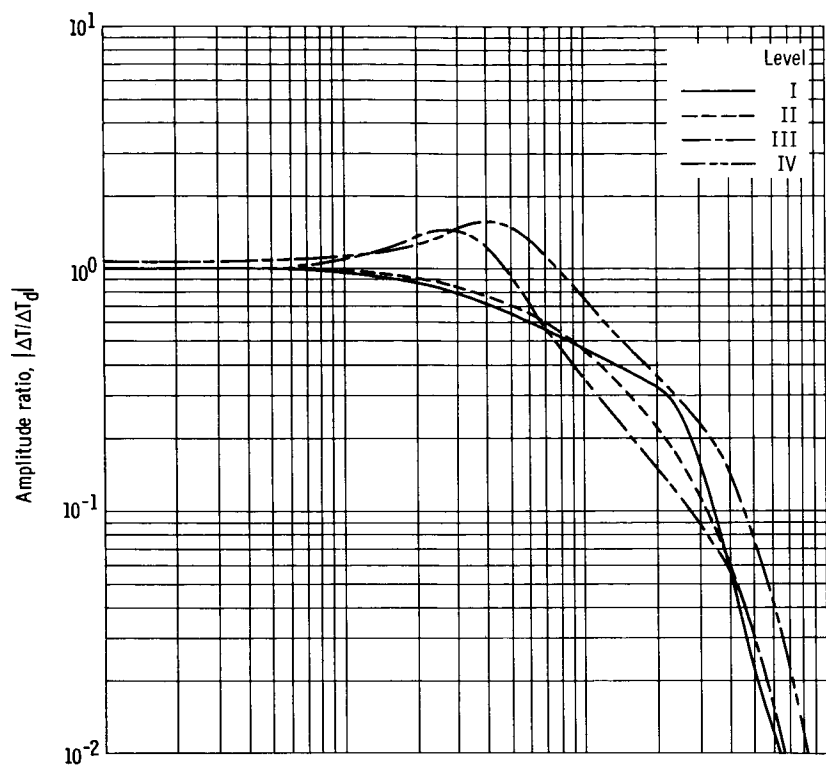Figure 5. – Operating level effects on open power loop without controller compensation at infinite reactor period.
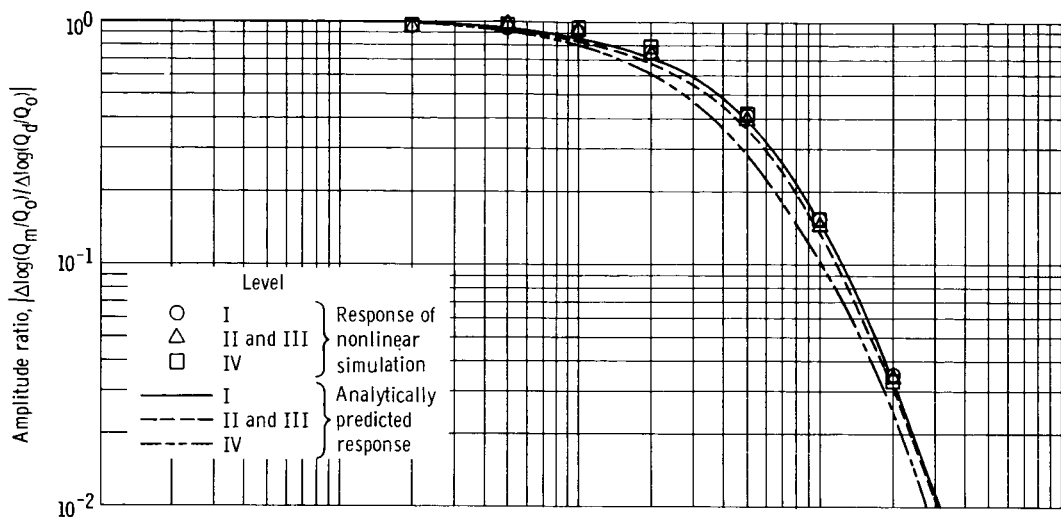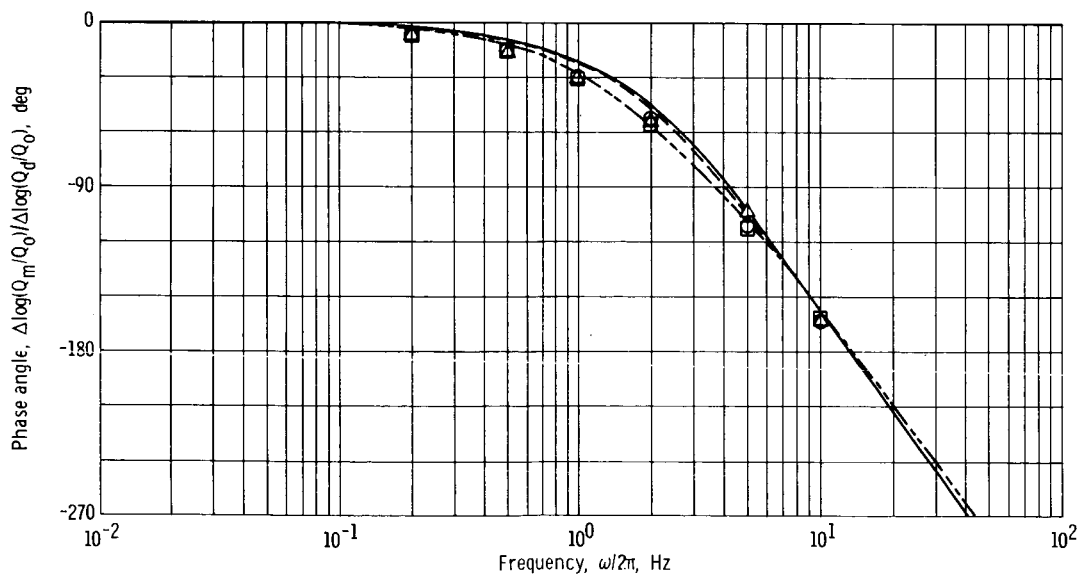
(a) Amplitude ratio.

(b) Phase angle.

Figure 6. - Closed-power-loop response at infinite reactor period with controller transfer function, $G_{c,p}(s) = 385\left[1 + s/25 + (s/25)^2\right]\Big/s(1 + s/100)^2$.
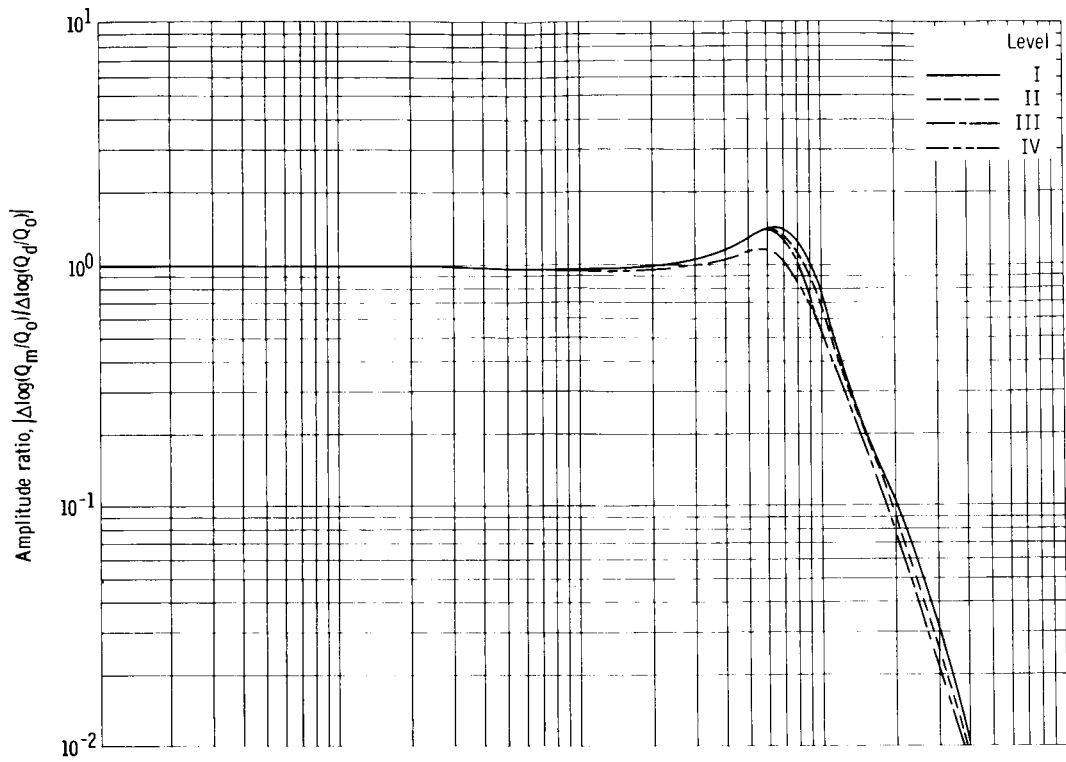
(a) Amplitude ratio.
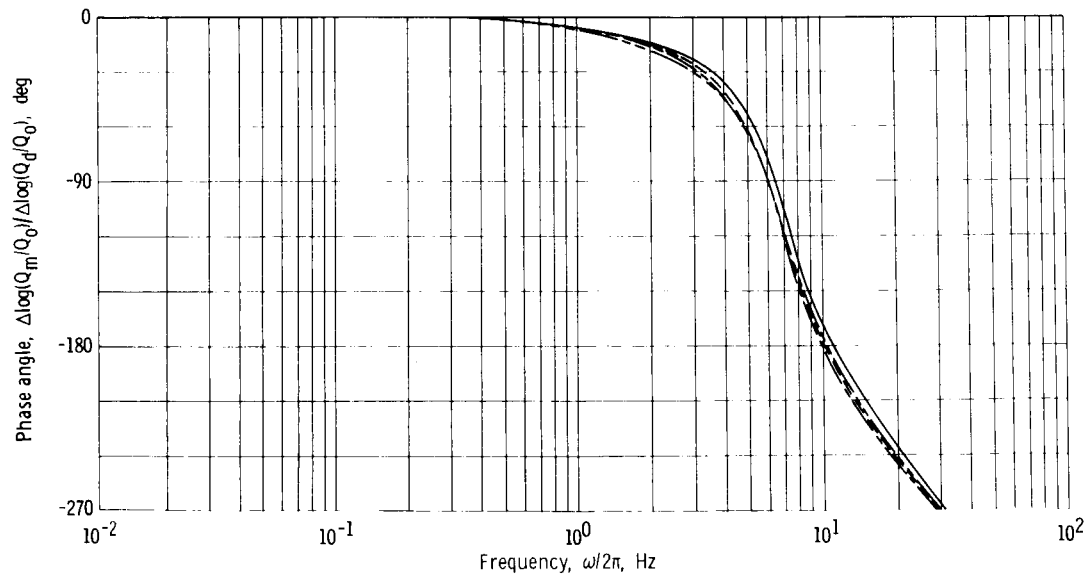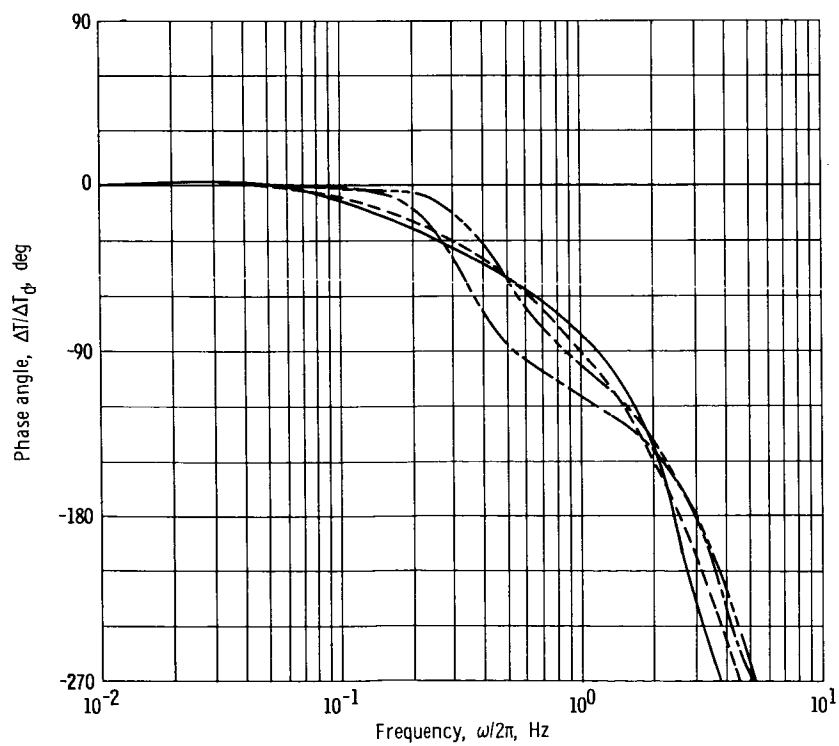
(b) Phase angle.

Figure 7. - Closed-power-loop response at 2-second reactor period with controller transfer function,

$$G_{c,p}(s) = 385\left[1 + s/25 + (s/25)^2\right]\Big/s(1 + s/100)^2.$$
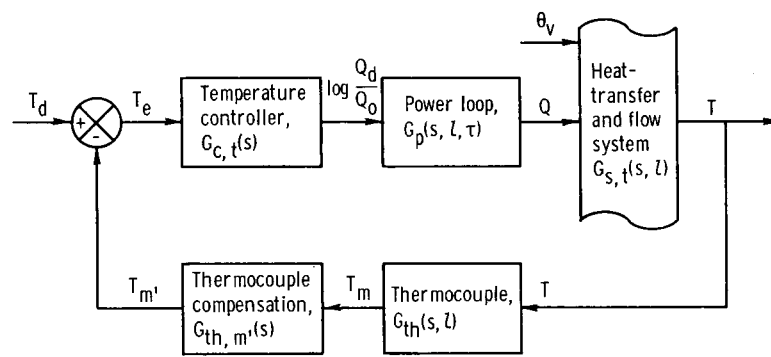
Figure 8. - Temperature control with inner power loop.
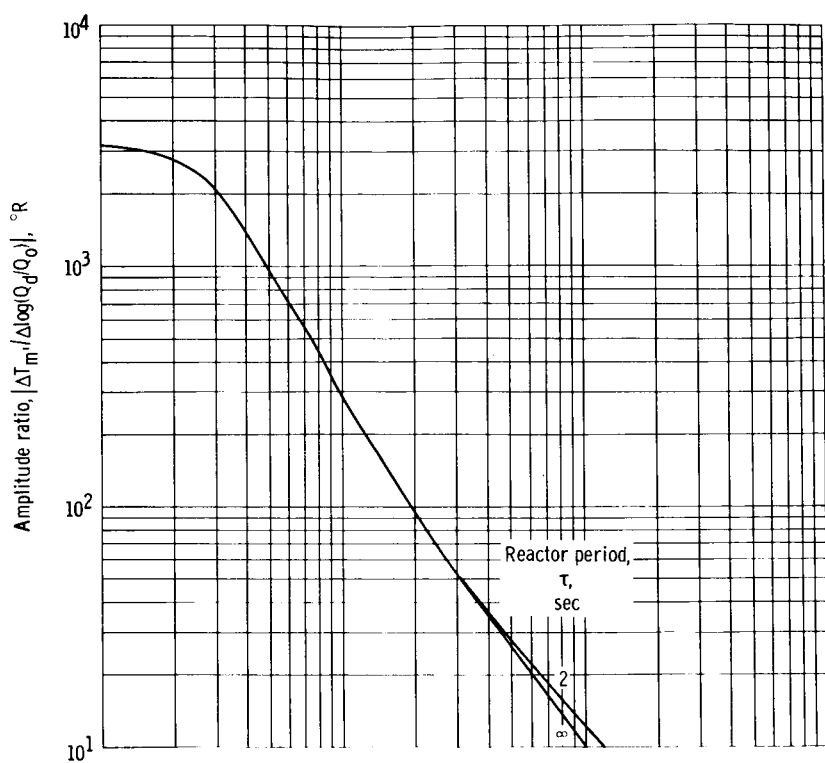
(a) Amplitude ratio.
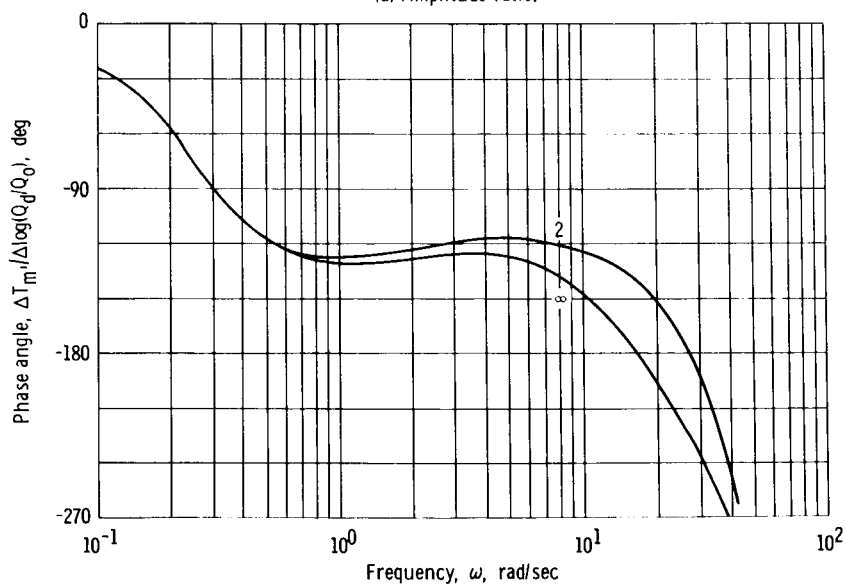
(b) Phase angle.

Figure 9. – Reactor period effects on open temperature and closed power loops at level III.
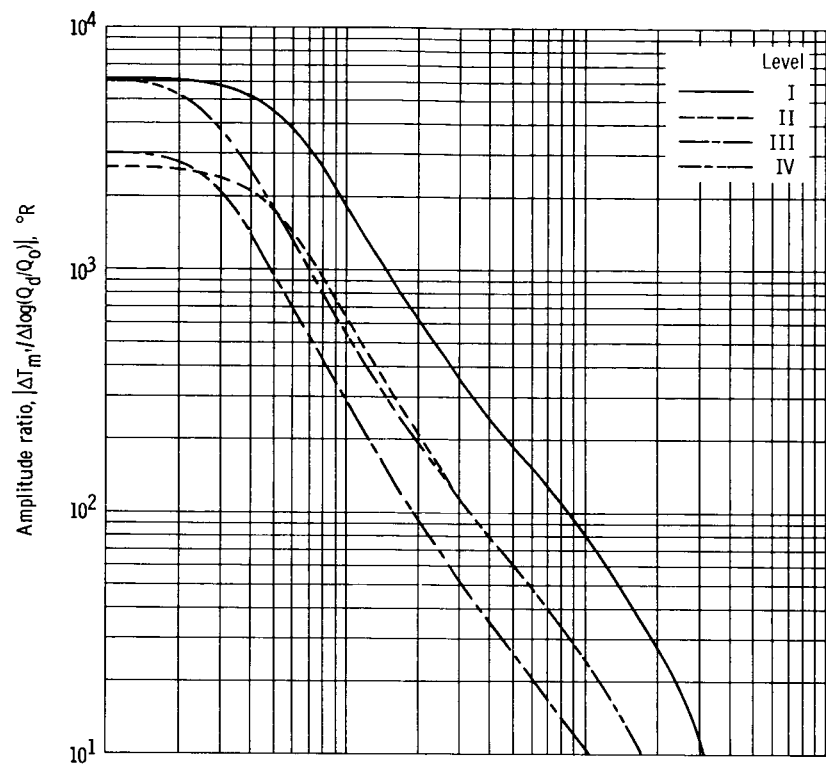
(a) Amplitude ratio.
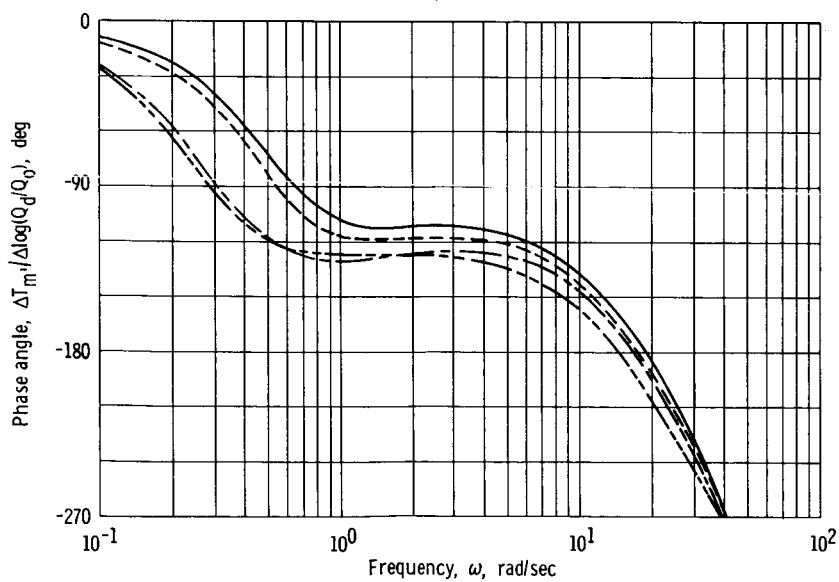
(b) Phase angle.

Figure 10. – Operating level effects on open temperature and closed power loops at infinite reactor period.

(a) Amplitude ratio.

Configuration

$G_{1,1}(s) = (1 + s)/s(1 + s/60)$
$G_{1,2}(s) = (1 + s/0.5)/s(1 + s/60)$
$G_{1,3}(s) = (1 + s/0.1)/s(1 + s/60)$
$G_2(s) = (1 + s/0.1)(1 + s/10)/s(1 + s/60)(1 + s/100)$
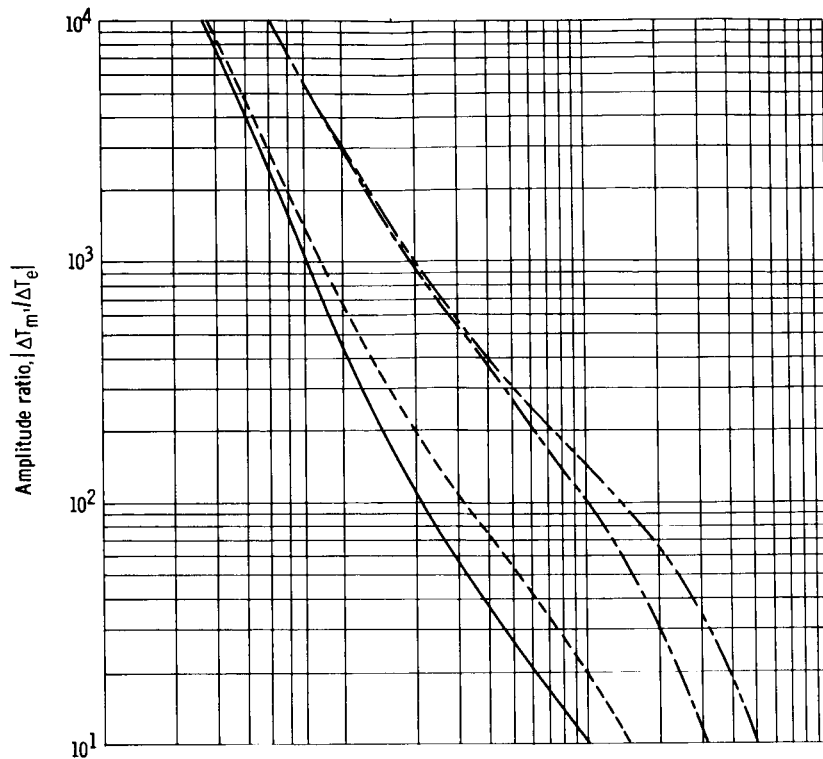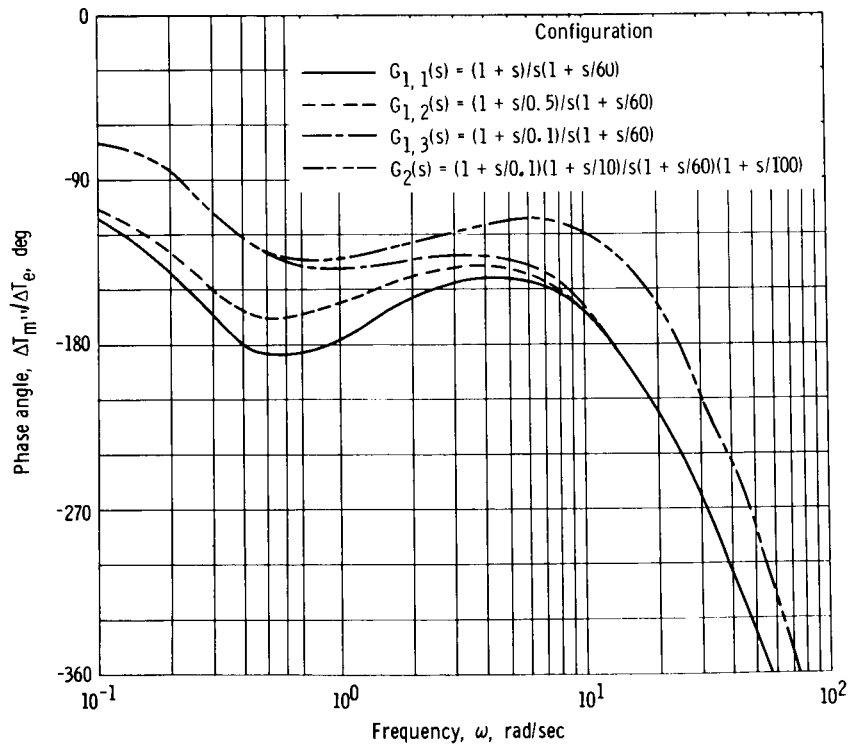
(b) Phase angle.

Figure 11. – Comparison of control configurations for use in control of temperature loop with inner-power loop. Open-loop response at level III and infinite reactor period.
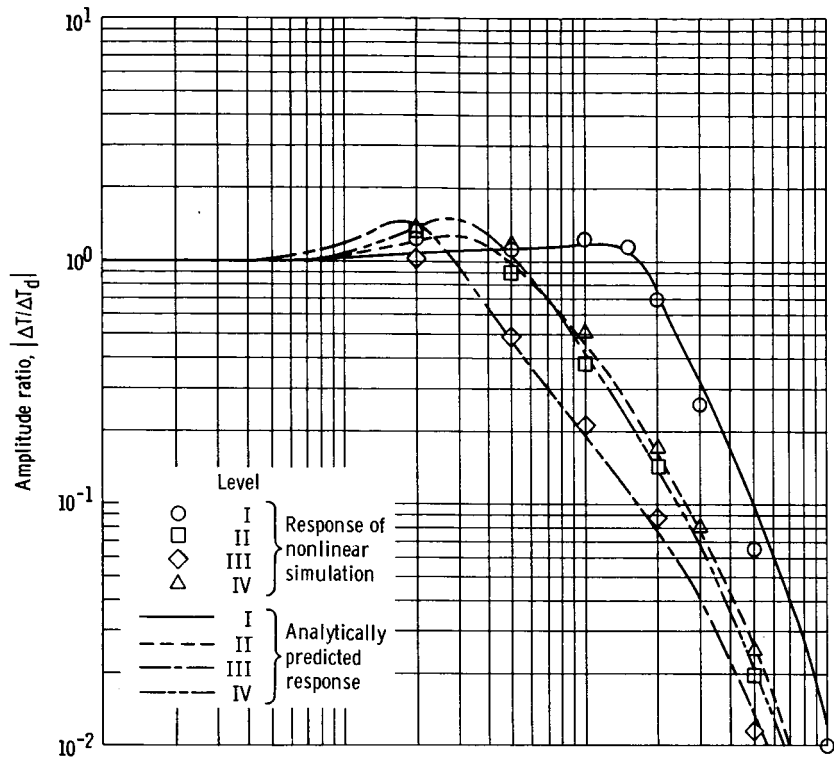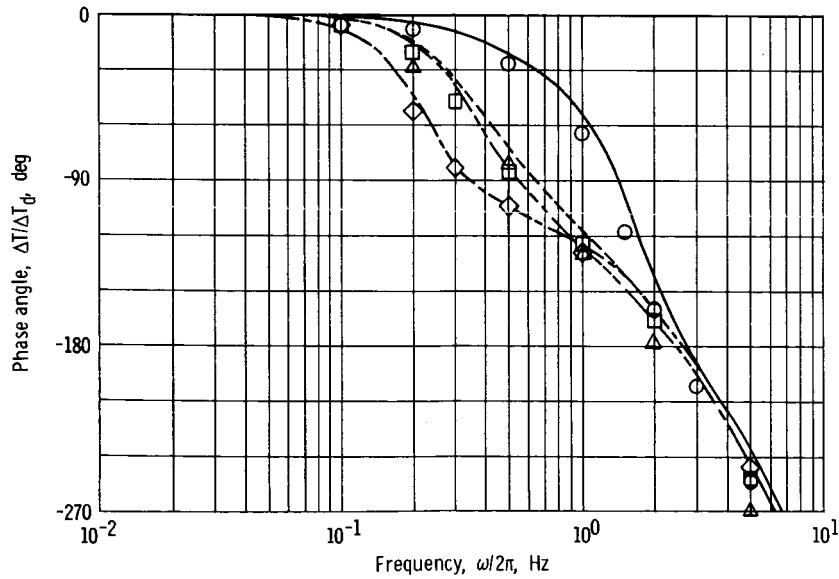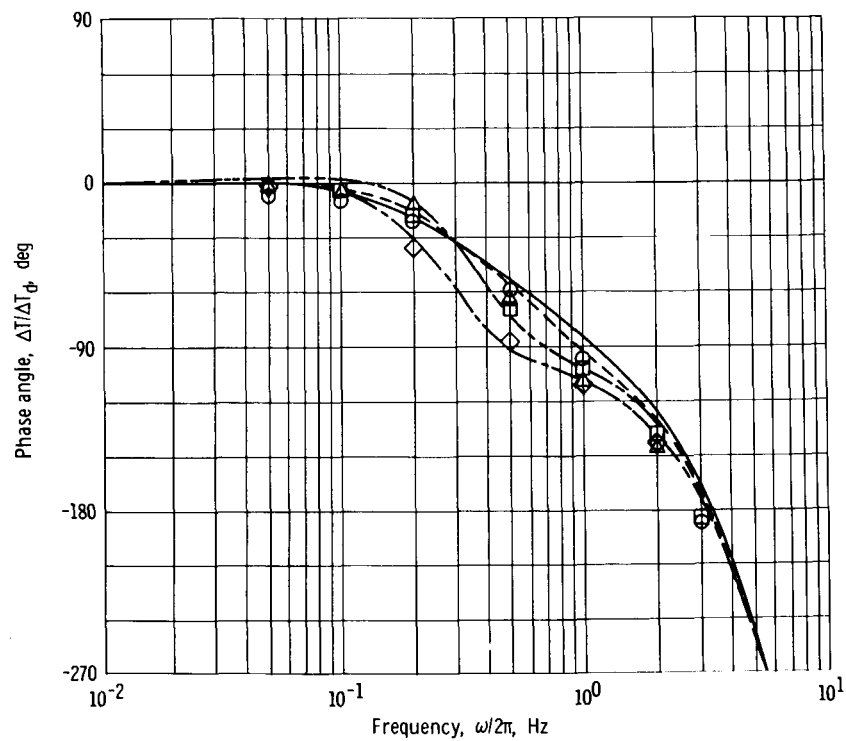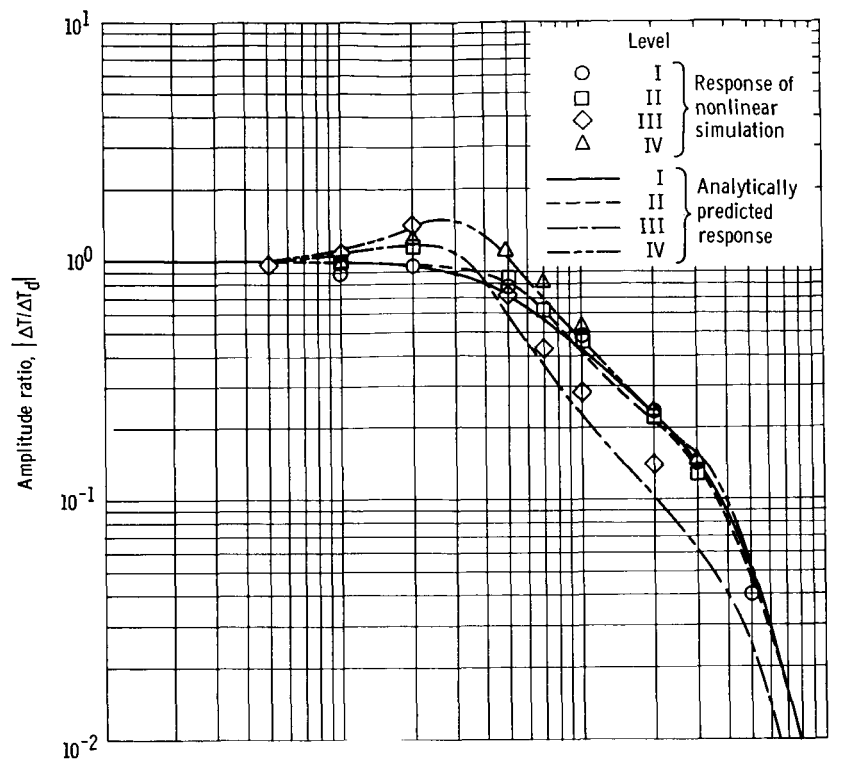
(a) Amplitude ratio.

(b) Phase angle.

Figure 12. - Closed temperature loop response at infinite reactor period with controller transfer functions, $G_{c,p}(s) = 385\left[1 + s/25 + (s/25)^2\right]/s(1 + s/100)^2$ and $G_{c,t}(s) = 6.5 \times 10^{-4}(1 + s/0.1)/s(1 + s/60)$.
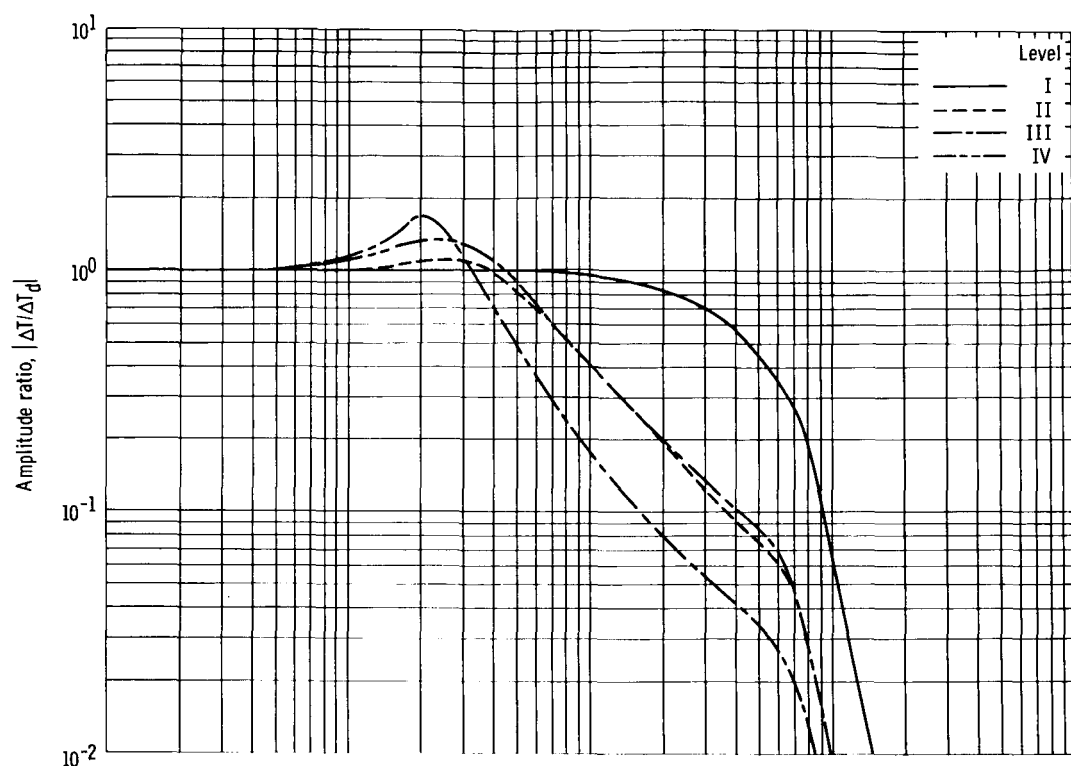
(a) Amplitude ratio.
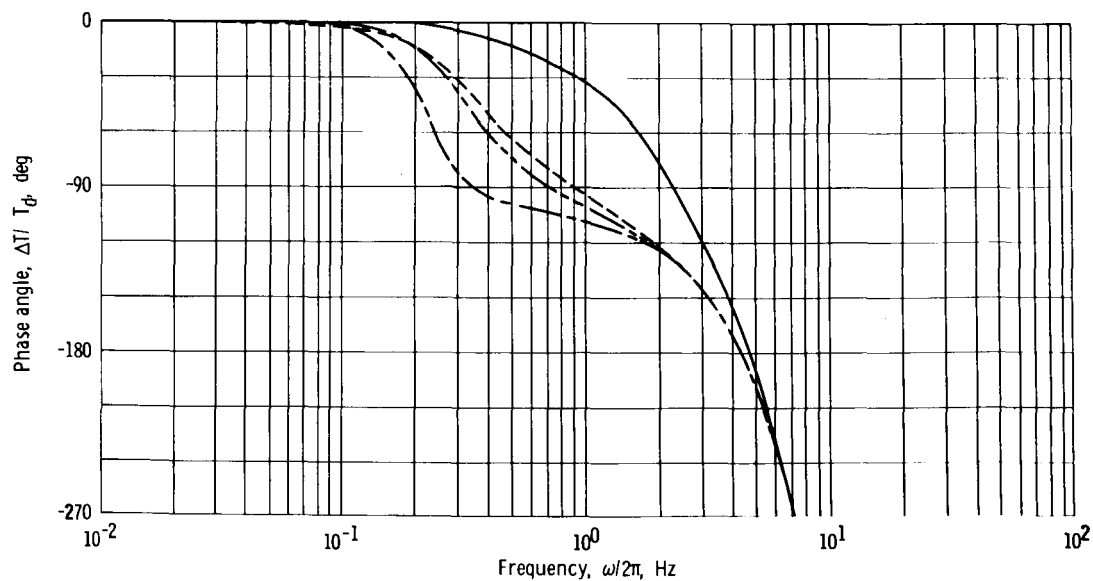
(b) Phase angle.

Figure 13. – Closed temperature loop response at 2-second reactor period with controller transfer functions, $G_{c,p}(s) = 385(1 + s/25 + (s/25)^2)/s(1 + s/100)^2$, $G_{c,t}(s) = 6.5 \times 10^{-4}(1 + s/0.1)/s(1 + s/60)$.
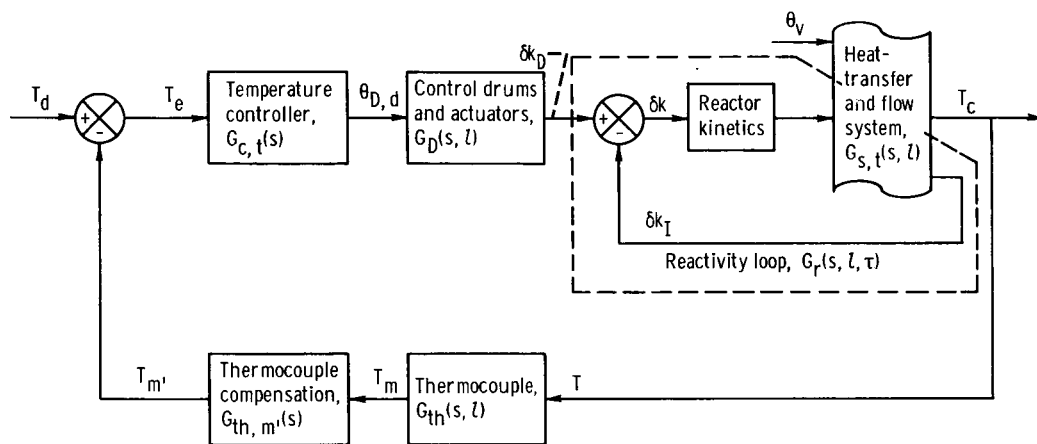
Figure 14. – Temperature control without power control loop.
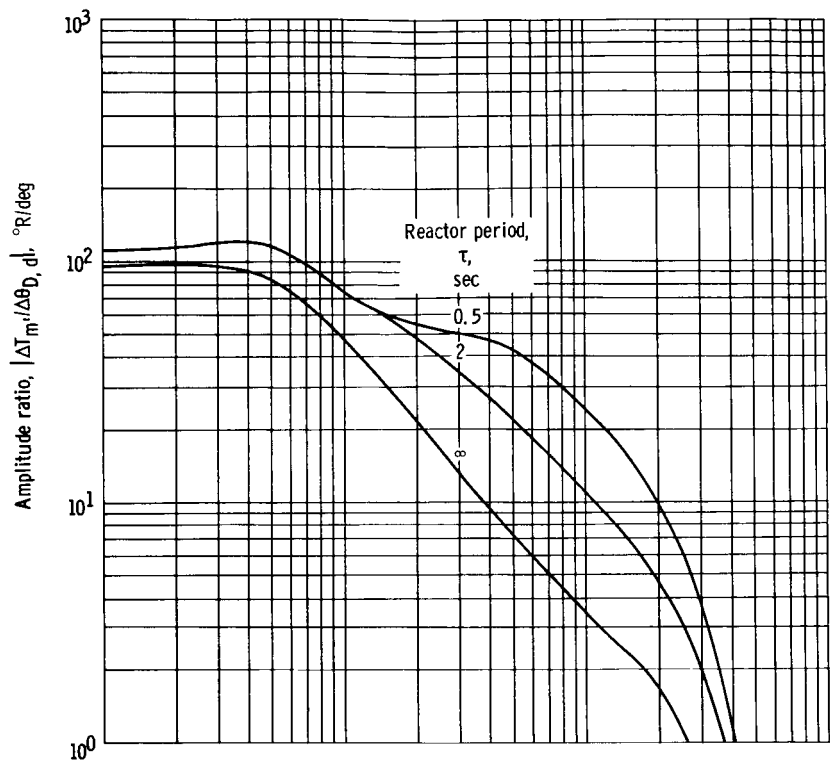
(a) Amplitude ratio.
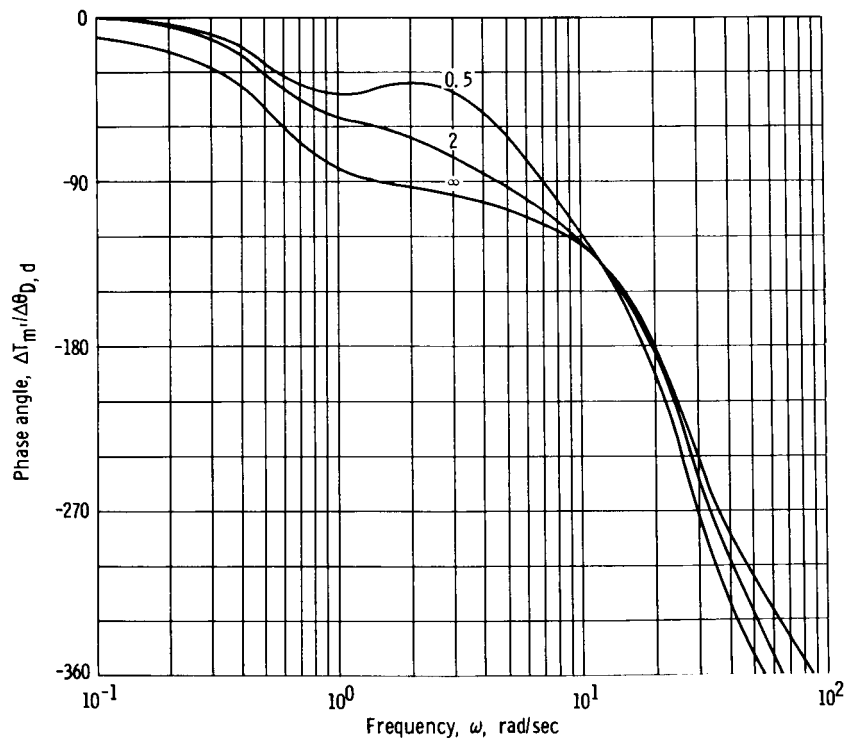
(b) Phase angle.

Figure 15. – Reactor period effects on open temperature loop at level I with thermo-couple compensation included.
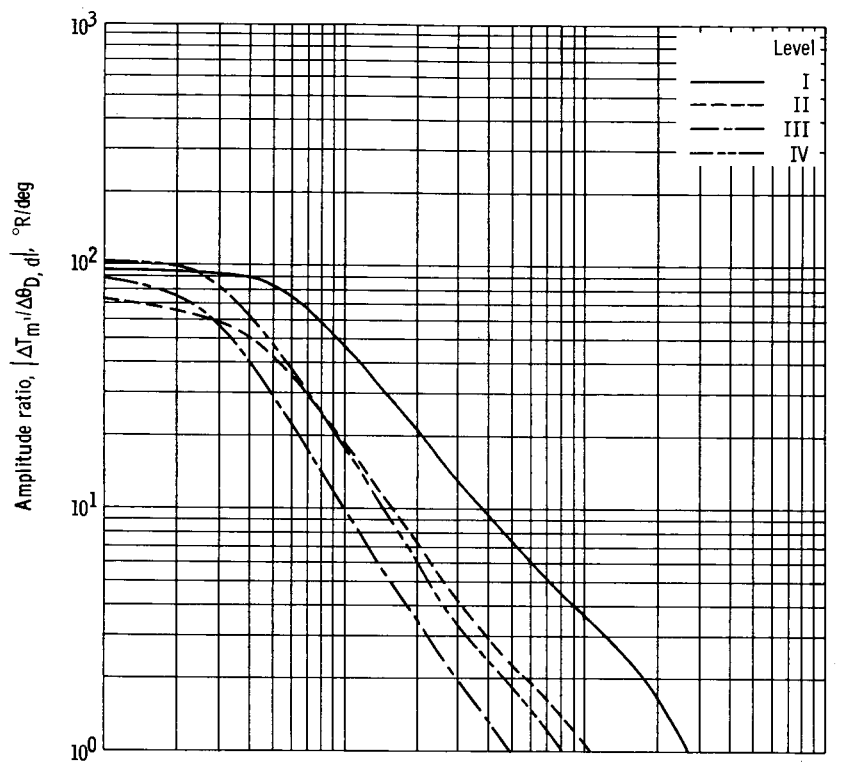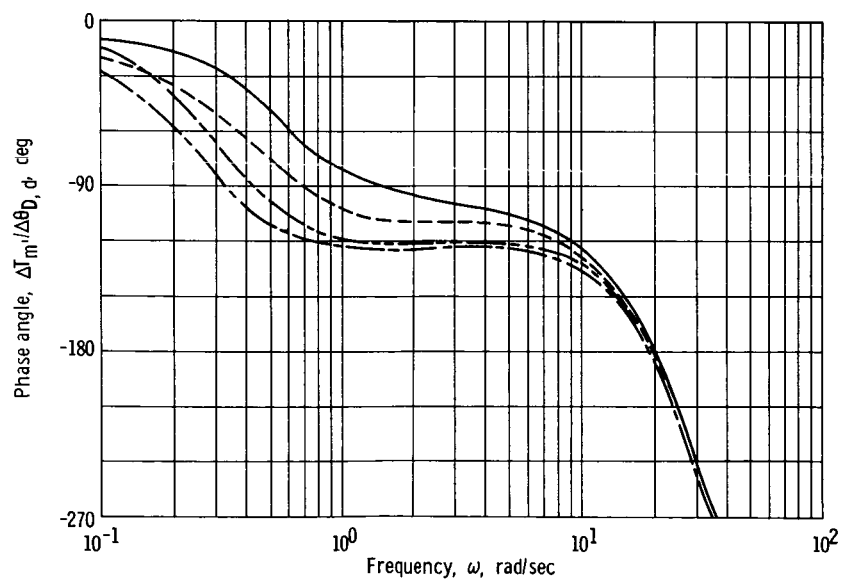
(a) Amplitude ratio.

(b) Phase angle.

Figure 16. – Operating level effects on open temperature loop at infinite reactor
period with thermocouple compensation included.
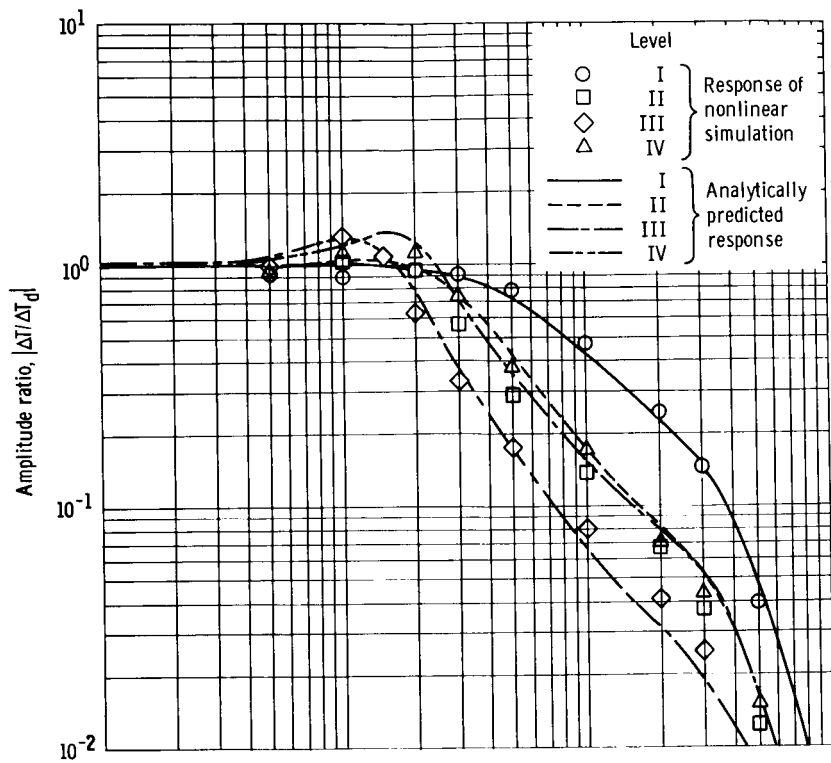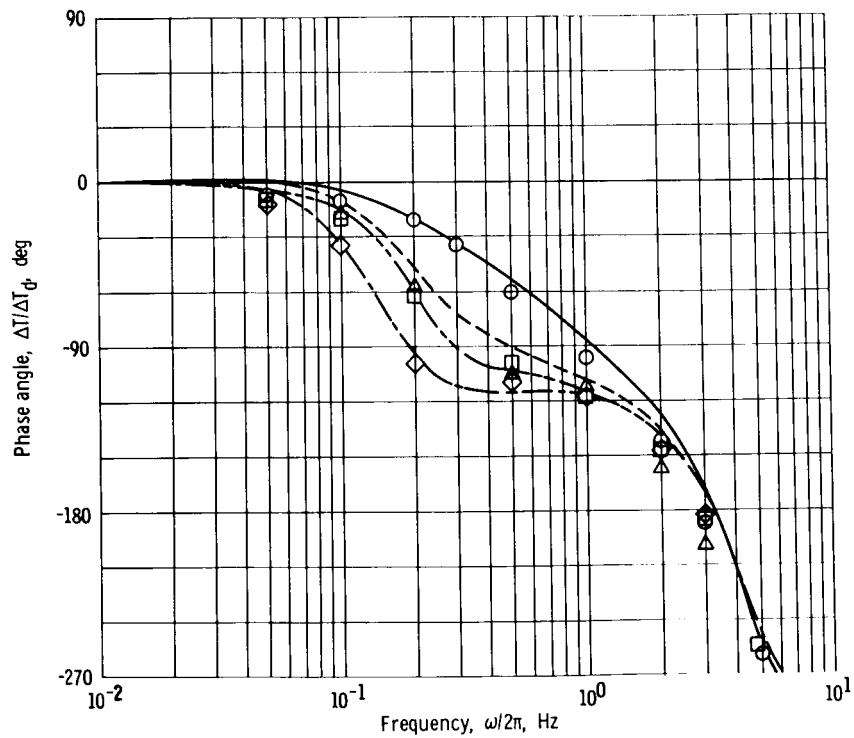
(a) Amplitude ratio.

(b) Phase angle.

Figure 17. – Closed-temperature-loop response at infinite reactor period with controller transfer function, $G_{c,t}(s) = 7.5 \times 10^{-3} (1 + s/0.1)/s(1 + s/60)$.

(a) Amplitude ratio.

(b) Phase angle.

Figure 18. – Closed temperature loop response at 2-second reactor period with controller transfer function, $G_{c,t}(s) = 7.5 \times 10^{-3} (1 + s/0.1)/s(1 + s/60)$.

(a) Amplitude ratio.

(b) Phase angle.

Figure 19. - Closed temperature loop response at infinite reactor period with controller transfer function, $G_{c, t}(s) = K_c(1 + s/0.1)/s(1 + s/60)$, where $K_c = -4.6 \times 10^{-5} P + 3.28 \times 10^{-2}$.
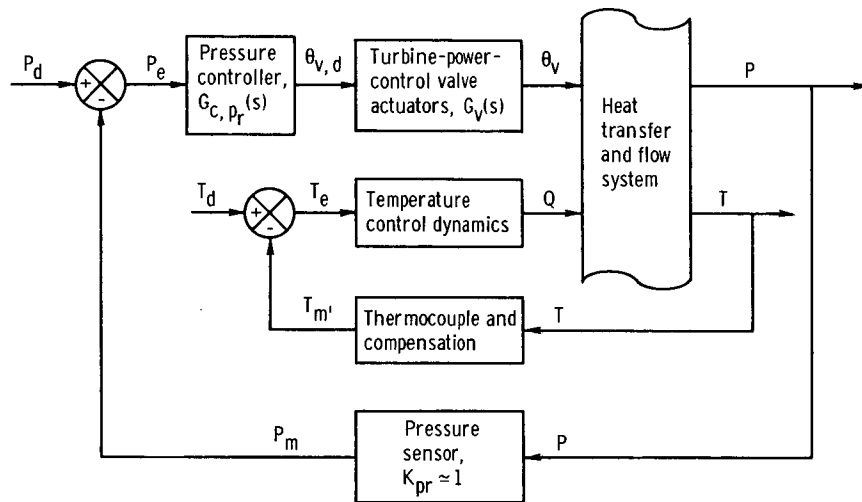
Figure 20. – Pressure control loop.

(a) Amplitude ratio.
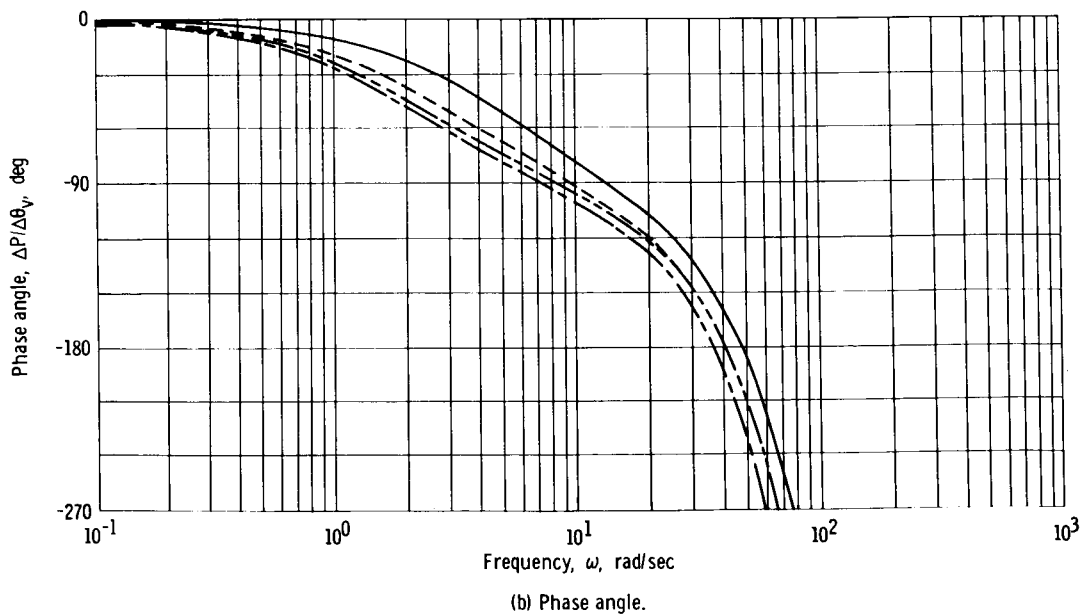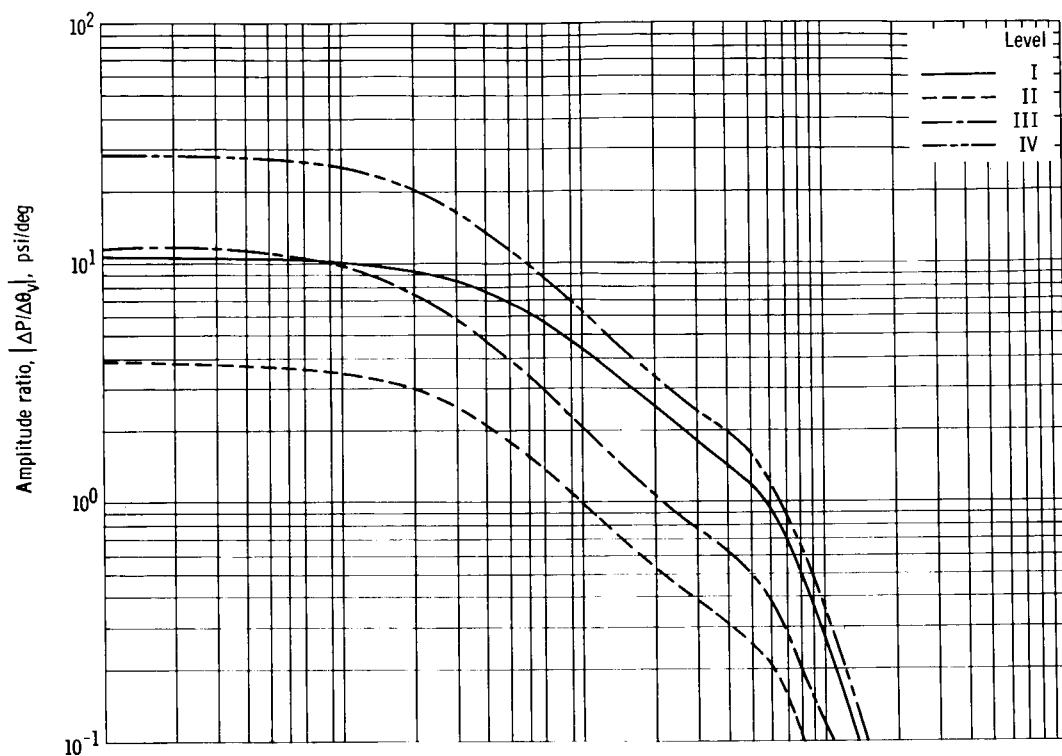
(b) Phase angle.

Figure 21. – Operating level effects on open pressure loop (excluding any controller transfer function) with constant exhaust-nozzle chamber temperature demand.

60
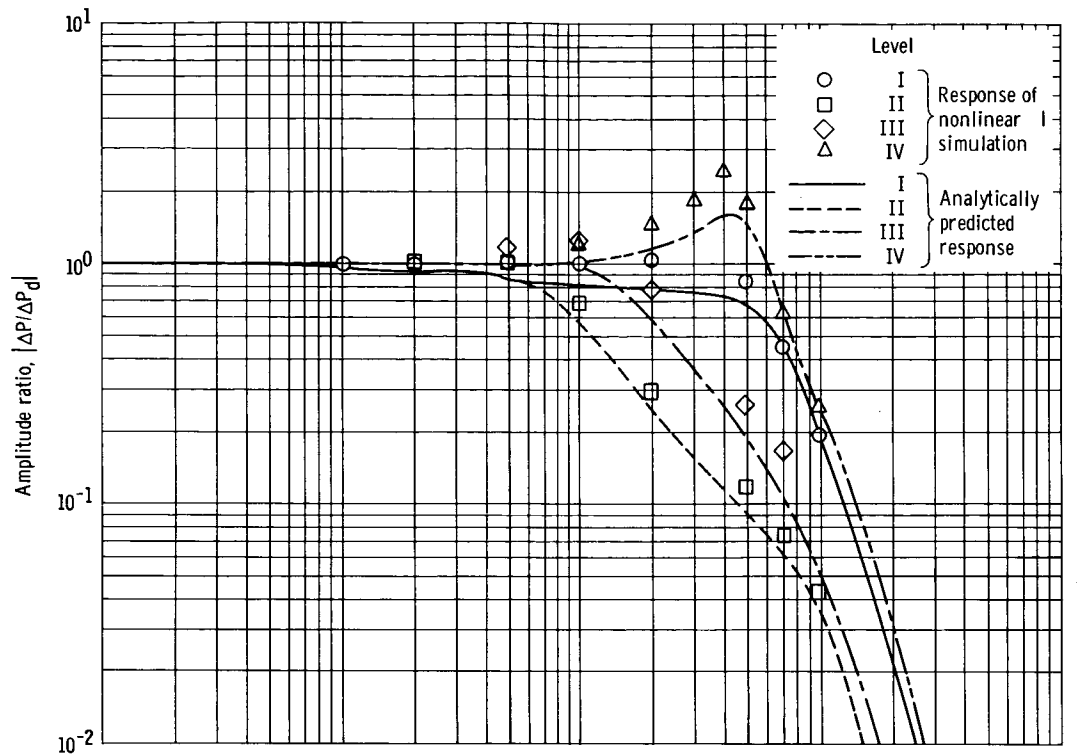
(a) Amplitude ratio.
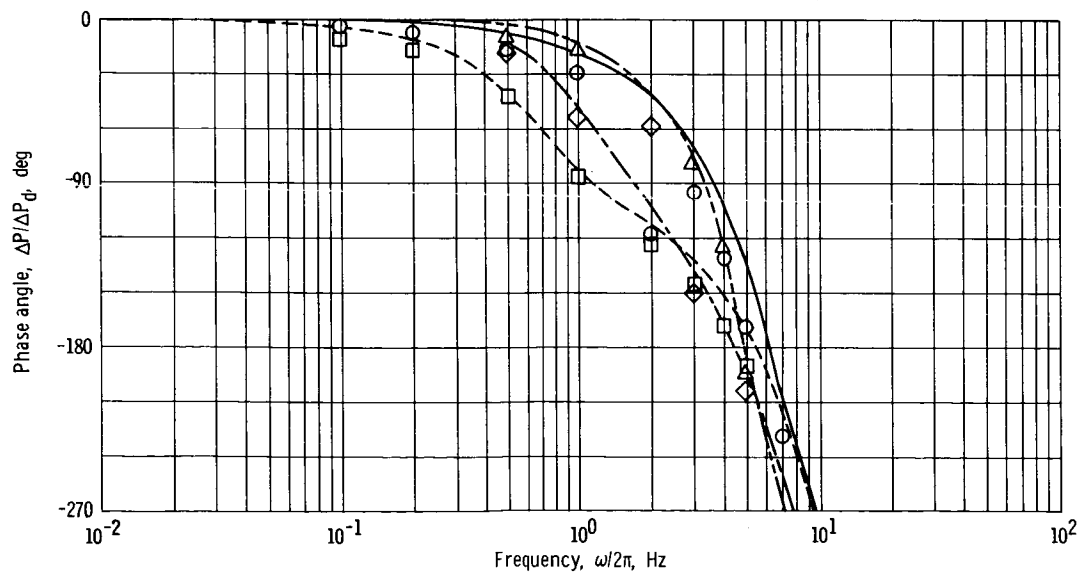
(b) Phase angle.

Figure 22. – Closed pressure loop response with controller transfer function, $G_{c,pr}(s) = 1.43(1 + s/5)/s(1 + s/100)$.
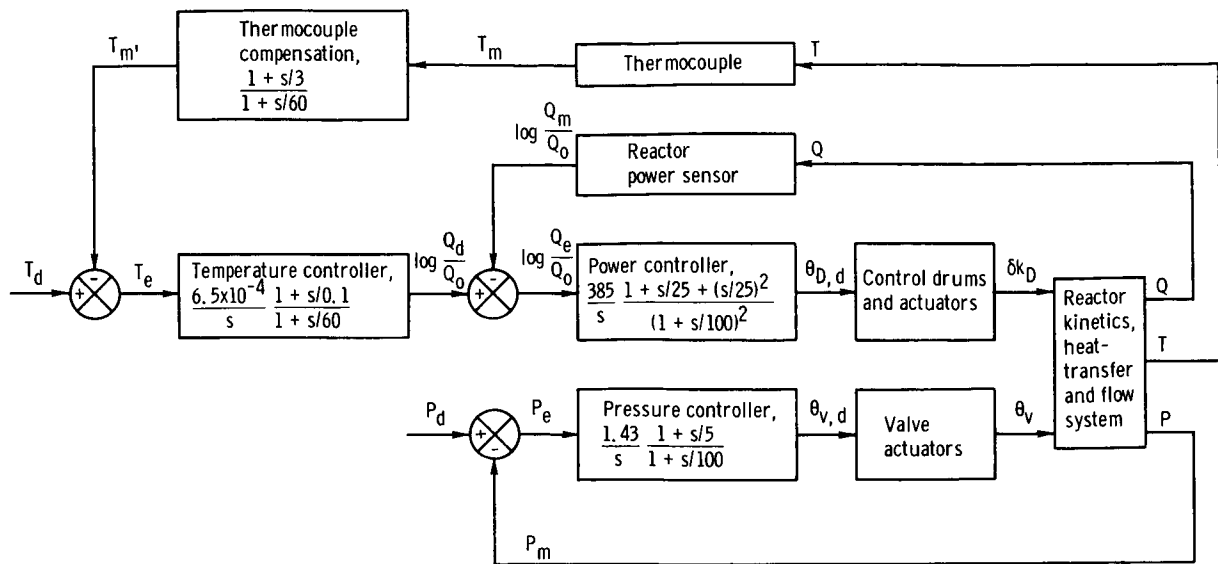
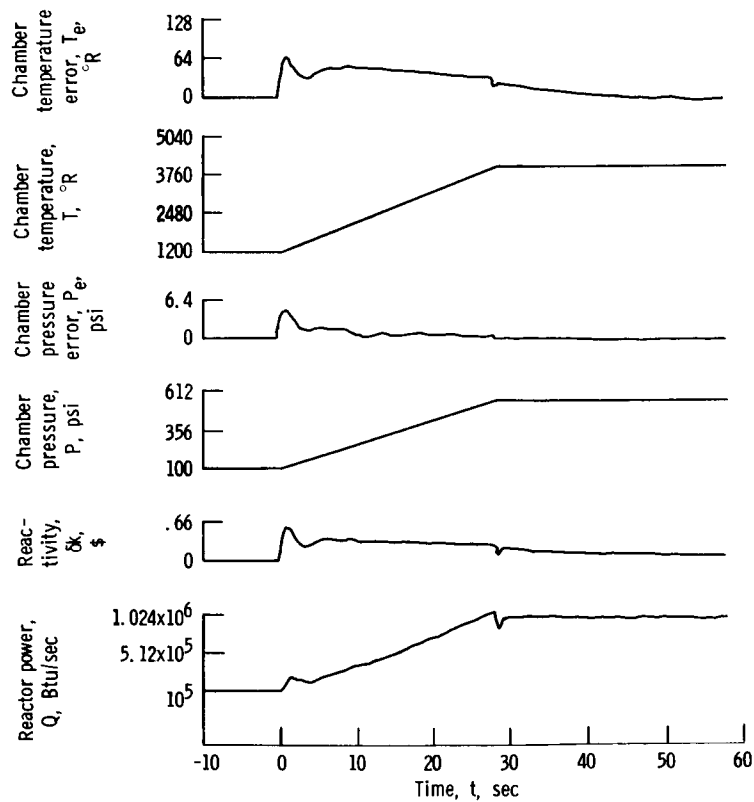Figure 23. – Engine control with use of power control loop.

Figure 24. – Controlled power range startup with reactor power control loop, where $T_d = 1250 + \int_0^{28.4} 100 \, dt$ and $P_d = 100 + \int_0^{28.4} 15.8 \, dt$.
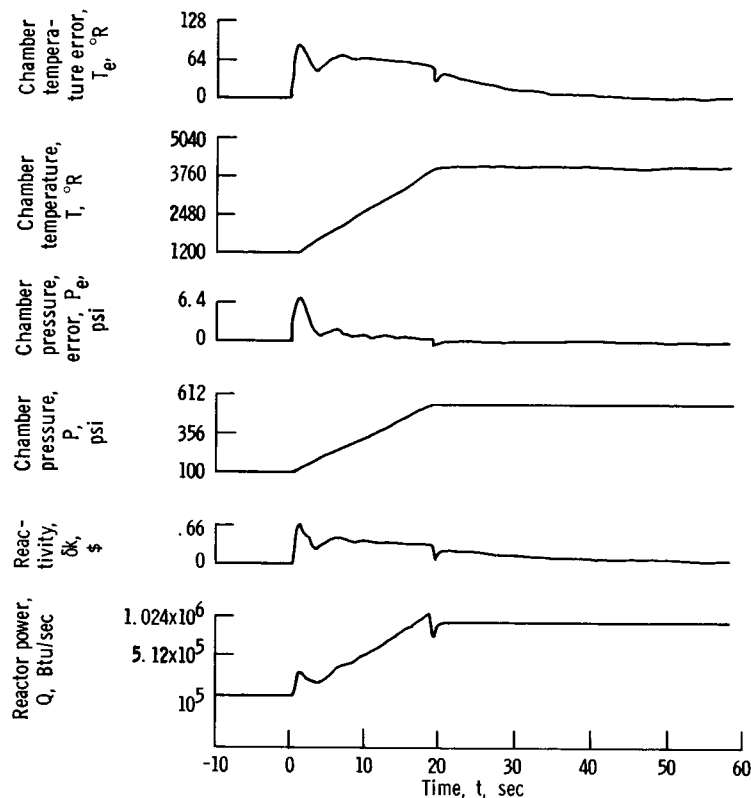
Figure 25. - Controlled power range startup with reactor power control loop, where $T_d = 1250 + \int_0^{18.9} 150\ dt$ and $P_d = 100 + \int_0^{18.9} 23.8\ dt$.
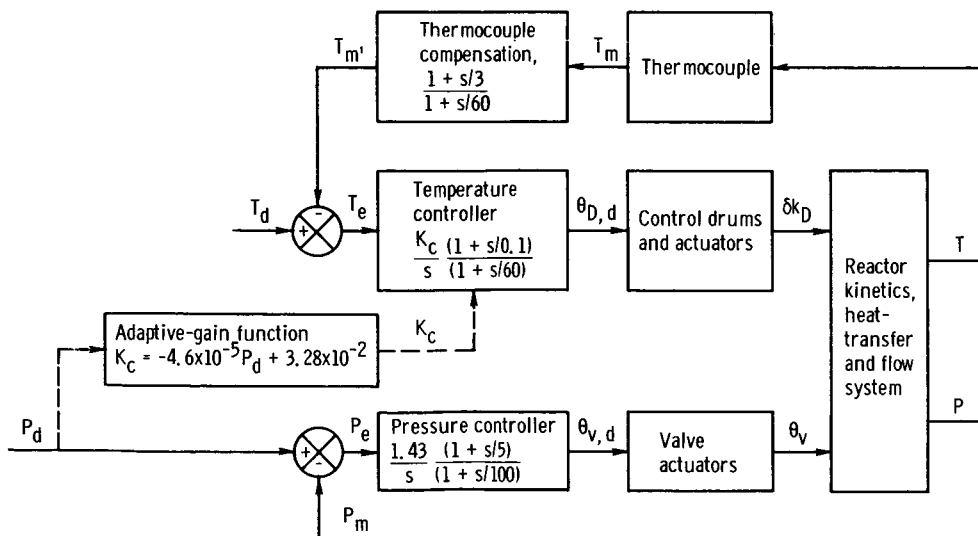

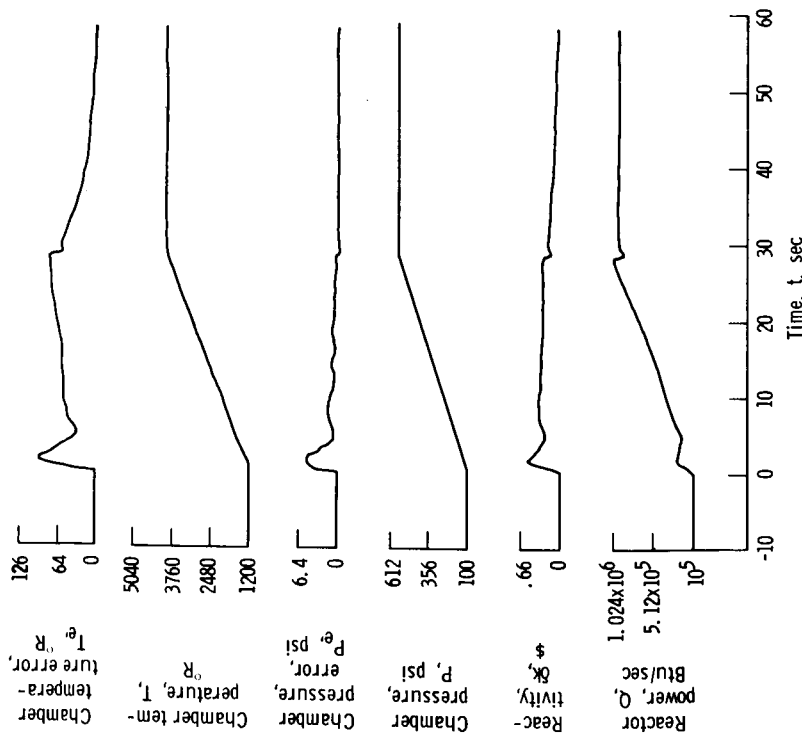Figure 26. - Engine control without power control loop.

Figure 27. - Controlled power range startup without reactor power control loop and with fixed-gain temperature control, where

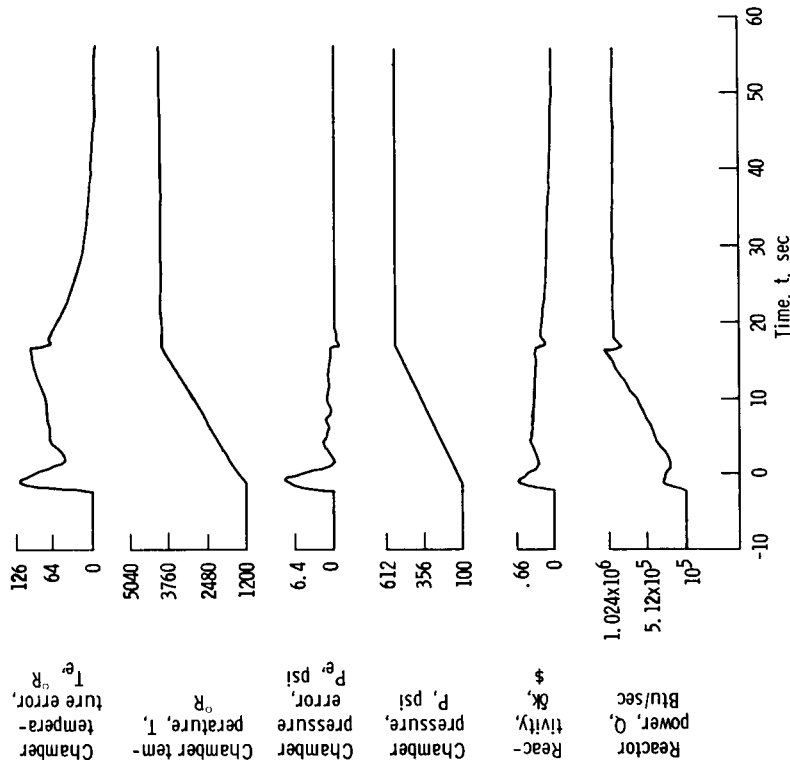$$T_d = 1250 + \int_0^{28.4} 100 \, dt \text{ and } P_d = 100 + \int_0^{28.4} 15.8 \, dt.$$

Figure 28. - Controlled power range startup without reactor power control loop and with fixed-gain temperature control, where

$$T_d = 1250 + \int_0^{18.9} 150 \, dt \text{ and } P_d = 100 + \int_0^{18.9} 23.8 \, dt.$$
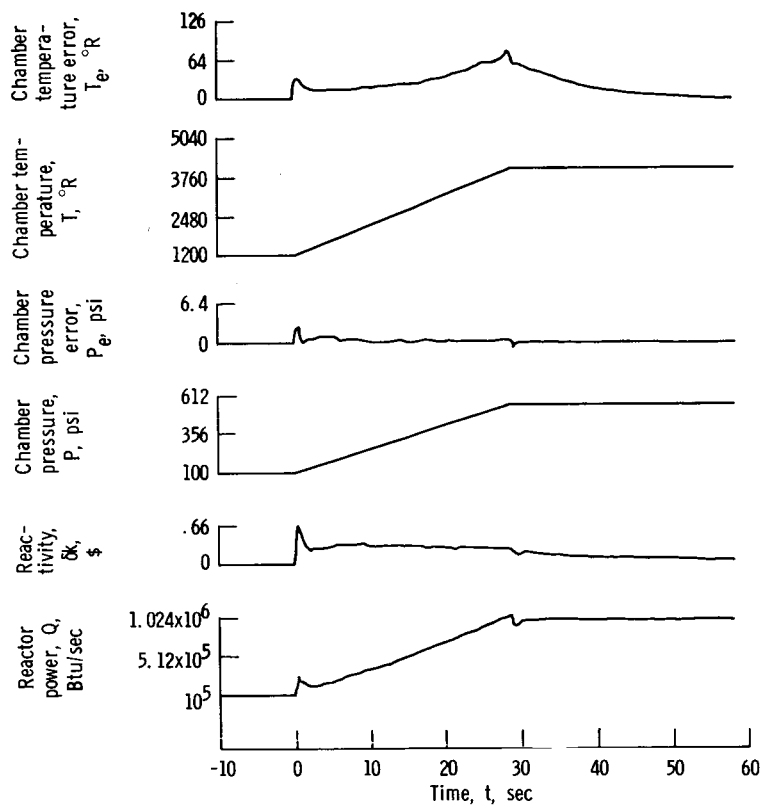
Figure 29. - Controlled power range startup without reactor power control loop and with adaptive-gain temperature control, where

$$T_d = 1250 + \int_0^{28.4} 100 \, dt \quad \text{and} \quad P_d = 100 + \int_0^{28.4} 15.8 \, dt.$$

"The aeronautical and space activities of the United States shall be conducted so as to contribute . . . to the expansion of human knowledge of phenomena in the atmosphere and space. The Administration shall provide for the widest practicable and appropriate dissemination of information concerning its activities and the results thereof."

—NATIONAL AERONAUTICS AND SPACE ACT OF 1958

NASA SCIENTIFIC AND TECHNICAL PUBLICATIONS

TECHNICAL REPORTS: Scientific and technical information considered important, complete, and a lasting contribution to existing knowledge.

TECHNICAL NOTES: Information less broad in scope but nevertheless of importance as a contribution to existing knowledge.

TECHNICAL MEMORANDUMS: Information receiving limited distribution because of preliminary data, security classification, or other reasons.

CONTRACTOR REPORTS: Scientific and technical information generated under a NASA contract or grant and considered an important contribution to existing knowledge.

TECHNICAL TRANSLATIONS: Information published in a foreign language considered to merit NASA distribution in English.

SPECIAL PUBLICATIONS: Information derived from or of value to NASA activities. Publications include conference proceedings, monographs, data compilations, handbooks, sourcebooks, and special bibliographies.

TECHNOLOGY UTILIZATION PUBLICATIONS: Information on technology used by NASA that may be of particular interest in commercial and other non-aerospace applications. Publications include Tech Briefs, Technology Utilization Reports and Notes, and Technology Surveys.

Details on the availability of these publications may be obtained from:

SCIENTIFIC AND TECHNICAL INFORMATION DIVISION

NATIONAL AERONAUTICS AND SPACE ADMINISTRATION

Washington, D.C. 20546